PULSATILE FLOW AROUND HEATED SEMI-CIRCULAR CYLINDER

DISSERTATION

Submitted in the partial fulfilment of the

requirements for the award of

INTEGRATED DUAL DEGREE

(Bachelor of Technology and Master of Technology)

in

CHEMICAL ENGINEERING

(Specialization in Hydrocarbon Engineering)

Submitted By

NEELESH BHALLA

(Enrollment No. 11210014)

DEPARTMENT OF CHEMICAL ENGINEERING
INDIAN INSTITUTE OF TECHNOLOGY ROORKEE
ROORKEE - 247667 (INDIA)

2016

CERTIFICATE

CANDIDATE'S DECLARATION

I hereby declare that this dissertation, entitled **"PULSATILE FLOW AROUND HEATED SEMI-CIRCULAR CYLINDER"** being submitted in the partial fulfilment of the requirement for the award of integrated dual degree **(IDD)** of **Bachelor of Technology in Chemical Engineering & Master of Technology in Hydrocarbon Engineering** in the Department of Chemical Engineering, Indian Institute of Technology (IIT) Roorkee, India, is an authentic record of my own work carried out under the supervision of **Dr. Amit Kumar Dhiman**, Associate Professor, Department of Chemical Engineering, Indian Institute of Technology (IIT) Roorkee India.

The matter embodied in this dissertation has not been submitted by me for the award of any other degree of this or any other Institute/University.

Dated: **NEELESH BHALLA**
Place: Roorkee **(Enrollment No. 11210014)**

SUPERVISOR'S DECLARATION

This is to certify that the above statement made by the candidate is correct to the best of my knowledge. This work is his original research performed under my supervision.

Dated:
Place: Roorkee

DR. AMIT KUMAR DHIMAN
Associate Professor
Department of Chemical Engineering
Indian Institute of Technology (IIT) Roorkee
Roorkee - 247667

ACKNOWLEDGEMENTS

First and foremost, praises and thanks to the Almighty, for his showers of blessings upon me.

I express my deep sense of gratitude and indebtedness to my revered guide **Dr. Amit Kumar Dhiman**, Associate Professor, Department of Chemical Engineering, Indian Institute of Technology Roorkee, India, for his continuous support, never ending inspirations and guidance, all blended with the personal touch throughout the duration of this work. His invaluable suggestions and thorough discussions have immensely contributed towards the completion of this work.

I take this opportunity to put on record my gratitude towards the Department of Chemical Engineering, Indian Institute of Technology Roorkee, for providing various facilities during course of the present investigation.

I would like to thank my colleagues/scholars, who worked in the same laboratory as I did, for their valuable suggestions and help as and when required.

Last but not least, I am grateful to my family members for their love, suggestions and moral support without which I would not have achieved this goal.

NEELESH BHALLA

PUBLICATION BASED ON THIS DISSERTATION

- Bhalla, N., & Dhiman, A.K. (2016). Pulsating flow and heat transfer analysis around a heated semi-circular cylinder at low and moderate Reynolds numbers. *Submitted to International Referred Journal.*
  (Submission attached herewith)

ABSTRACT

A numerical analysis was carried out to examine the effect of pulsating flows around a semi-circular heated cylinder placed in a horizontal confined empty channel. The heat transfer induced as an outcome of non-zero mean sinusoidally varying flow past a semi-circular cylinder was investigated. For this purpose, computations are carried out for the following range of parameters: wall confinement (or blockage ratio, β) = 25%; Prandtl number (Pr) = 7 (water as a working fluid); Reynolds number (Re) = 10-100; Strouhal number (St) = 0-2; and amplitude of oscillation (A) = 0-0.6. The flow is numerically investigated by solving the continuity, momentum and energy equations using the finite volume method–based solver Ansys Fluent. Results in terms of total drag coefficient and Nusselt number have been presented and discussed. The nature of flow for each considered case is reported. Also the flow (streamlines) and thermal (isothermal contours) patterns have been analyzed. The maximum augmentations of about 22% and 10% were obtained in drag coefficient and Nusselt number, respectively.

Keywords

Semi-circular cylinder; Pulsating flow; Confined flow; Strouhal number; Amplitude of oscillation and Forced convection.

CONTENTS

LIST OF FIGURES

LIST OF TABLES

NOMENCLATURE

Symbol	Parameter	Unit
English Symbols		
A	amplitude of oscillation for axial inlet velocity	dimensionless
Cp	heat capacity	$J.kg^{-1}.K^{-1}$
C_D	total drag coefficient	dimensionless
D	diameter	m
f	pulsating frequency	s^{-1} (or Hz)
G	gap ratio	dimensionless
Gr	Grashof number	dimensionless
h	heat transfer coefficient	$W.m^{-2}.K^{-1}$
H	channel height	m
k	thermal conductivity of the fluid	$W.m^{-1}.K^{-1}$
K_C	Keulegan–Carpenter number	dimensionless
L	channel length	m
L_d	downstream length	m
L_u	upstream length	m
n	power-law index	dimensionless
Nu	average Nusselt number	dimensionless
p	pressure	$N.\ m^{-2}$
Pr	Prandtl number, $Pr = (\mu Cp)/k$	dimensionless
q_s	heat flux on the surface of the cylinder	$W.m^{-2}$
Re	Reynolds number, $Re = (\rho DU/\mu)$	dimensionless
Ri	Richardson number	dimensionless
N_S	Stokes number	dimensionless
St	Strouhal number	dimensionless

t	time	s
T	temperature	K
U	average velocity	m/s
U_x, U_y	x- and y-components of the velocity	m/s
x,y	horizontal and vertical coordinates	m
Greek Symbols		
α	thermal diffusivity, $\alpha = k/(\rho\ Cp)$	$m^2.s^{-1}$
β	wall confinement	dimensionless
δ	size of the CV clustered around a semi-circular obstacle	m
μ	dynamic viscosity	Pa.s
ρ	density of the fluid	$kg.m^{-3}$
τ	time period of oscillation	s
ω	pulsatile free stream frequency	s^{-1} (or Hz)
ω_c	cylinder oscillations frequency	s^{-1} (or Hz)
Subscripts		
c	critical value	---
w	surface of a semi-circular obstacle	
∞	inlet condition	

Dedicated to IIT Roorkee.

CHAPTER 1. INTRODUCTION & LITERATURE REVIEW

The growing demand of better and effective cooling techniques in order to achieve a higher rate of heat exchange with minimum frictional loss is prominent in chemical and related process industries. Flow of fluids around a long semi-circular obstacle has been a research topic of much interest for years. Vortex-shedding phenomenon is created as a consequence of flow hindrance from the cylindrical-shape bodies, thus causing pressure disturbances around the bluff body as well as vibration. Study of fluid flow over a semi-circular cylinder finds application in flow over tubes in heat exchangers, air flow past a bundle of pipes in plant, transmission cables with conductors, offshore structures exposed to ocean waves, chimney stacks, gusting of wind, ocean currents past pipelines and risers, total artificial lung devices and many others.

In recent years, Chandra and Chhabra [1] numerically investigated the heat transfer due to forced convection from a semi-circular cylinder immersed in unconfined flowing Newtonian fluids. The study elucidates the influence on global flow as well as heat transfer characteristics caused as a consequence of varying the Prandtl number (Pr = 0.72-100) and Reynolds number $(0.01 \le \mathrm{Re} \le 39.5)$. Also, the study explored the functional dependence of drag coefficients (both individual and total) on Re. In another similar study, Chandra and Chhabra [2] explored the variation of Nusselt number (*Nu*) along with the drag coefficient (C_D), this time incorporating the power law fluids into the system, for the following range of control parameters: $0.01 \le \mathrm{Re} \le 30$; $0.2 \le n$ (power-law index) ≤ 1.8 and $1 \le \mathrm{Pr} \le 100$. The authors reported a decrease in rate of heat transfer with gradual increase in *n* at fixed Pr and Re, the effect being appreciable at low Re and almost diminished with increase in Re. Later, as an addition to this work, Chandra and Chhabra [3] performed a study in the laminar vortex shedding regime for another set of conditions that were: $40 \le \mathrm{Re} \le 140$; $0.7 \le \mathrm{Pr} \le 50$; and $0.2 \le n \le 1.8$. It was observed that in case of shear-thinning fluids ($n < 1$), the effects of *n*, Re and Pr were more prominent than that in case of shear-thickening fluids ($n > 1$).

Kumar and Dhiman [4] worked on numerical simulation of incompressible Newtonian forced flow and heat transfer characteristics of a long heated semi-circular obstruction in a confined channel. For this purpose, the range of Re studied was 1-40 while the blockage ratio (β) varied in range of 16.67–50%, the working fluid being air. The study identified that the C_D values were greater than the corresponding unconfined flow situation. Also for the confined flow at appropriate set of values of dimensionless parameters, the C_D values in case of semi-circular cylindrical obstruction were found to be higher than that in case of a complete cylindrical obstruction. The study identified the correlations of average *Nu*, C_D and wake length. Even for the case of power law fluids, forced convection around a confined heated semi-circular cylinder has been numerically investigated by Kumar et al. [5]. The power-law index ranged between 0.2-1.8 with blockage ratio being 25%. The study was carried out for Pr=50 with Re=1-40. Upon increasing Re, the overall heat transfer rate increased with the study reporting a maximum enhancement of 47% in heat transfer in comparison to Newtonian fluids. Finally correlations were developed for *Nu*, C_D and wake length for the cases of studied Re and *n*.

1.1. Pulsatile flow

In recent times, amongst the newer active heat transfer augmentation schemes, the practice of incorporating forced pulsations into the incoming fluid (as it enters the channel) is gaining popularity. There exist many situations where heat is being practically transferred using forced pulsatile flow conditions. For instance, a few amongst the diverse applications of this technique include improved designs of chemical reactors and enhanced performance of heat exchangers using reciprocating pumps induced pulsatile flow. Other applications include studies on fluid transport involved in the animal cardiovascular systems, design of electronic cooling systems and the use of probes based on diffusion controlled electrode reactions to study flow transients. It has been identified that several researchers have been working in direction of oscillating (pulsating) flows. After all, the idea of heat transfer augmentation using forced pulsations is not relatively new.

Motivated by the idea of total artificial lung (TAL) that is envisioned for better gas exchange, Qamar et al. [6] investigated the flow around an oscillating cylinder in a pulsatile flow environment. Both the cylinder oscillations (frequency ω_c) as well as the pulsatile free stream velocity (frequency ω) were taken into account for the same. The authors defined the frequency of the oscillating cylinder by means of Keulegan–Carpenter number ($K_C = U/(D\omega_c)$) while keeping the pulsatile free-stream velocity fixed, for all cases considered, by imposing $\omega/K_C = 1$. Corresponding to the operating conditions of the TAL, the authors examined the following range of parameters: 5<Re<20; 0.33< K_C <1; and 0.5*D*<cylinder oscillation amplitude<*D*. The drag coefficient values were reported to decline at higher amplitudes and lower K_C. The study went on to quote a maximum rise of 246% in vorticity for every Re by increasing the amplitude and decreasing the K_C simultaneously, thus hinting towards enhanced mixing by the proposed TAL design.

Amongst the significant works available in the direction of pulsatile flow around bluff bodies, Al-Sumaily and Thompson [7] examined the changes to the heat transfer and flow induced by a steady and sinusoidally varying (with non-zero mean) flow past a cylindrical bluff body. Two configurations have been studied using separate approaches for each: (1) cylinder mounted in a horizontal empty channel making use of the incompressible Navier–Stokes equations; and (2) cylinder mounted in a horizontal porous-material filled channel bringing in use the Darcy–Brinkmann–Forchheimer momentum and the two-equation energy *LTNE* models. The study identifies the effects of the pulsation frequency (*St*) and the amplitude (*A*) on the heat transfer at various Re (= 1–250) for different types of porous materials keeping the structural properties constant. Transition from initial steady to unsteady wakes was reported for the non-filled (empty) channel as the Re grew. Depending upon the values of oscillation amplitude, Re and the forcing frequency, two different wake structures, namely quasi-periodic and fully periodic shedding, were observed for the time-dependent case. On the other hand, as a consequence of the dampening caused by the presence of the porous medium, highly stable flows resulted with no significant (extended) wakes, both in front as well as behind the cylinder.

In another totally different attempt to study flow of blood in a TAL, Lin et al. [8] designed an experimental apparatus. A prototype TAL, that serves as a bridge towards lung transplantation, comprises of cylindrical fibers (hollow) through which the air (rich in oxygen) and the blood (poor in oxygen) flows around. The study focused on the velocity flow profiles around these fibres bringing in use the numerical simulations as well as the particle image velocimetry (PIV) experiments. These fibres were modelled as a 5 cm long cylinder with a diameter of 0.05 cm for the purpose. In order to analyze the mechanism of flow around the cylinder, a low speed water tunnel was designed. A linear actuator generated flow across the tunnel as it could mimic the flow in a TAL. The study went on to summarize the behind-the-cylinder vortex formation phenomenon for a range of Stokes numbers (N_S) varying from 0.18 to 0.37, at three different Re (1, 3 and 5). Also, it was identified that vortex formation was favored at high values of Re and N_S. Motivated by the need to optimize the mechanical impedance of the fluid as well as the gas transfer in a total artificial lung, Lin et al. [9], in an experimental setup consisting of two cylinders, studied the pulsatile flow for different geometric arrangements. In contrast to the steady flow, for pulsatile flow the vortex formation occurred at low Re values. Also, the degree of dependence of vortex structure on Re and Stokes number as well as the geometric arrangement of the cylinders was found to be strong.

In yet another attempt to investigate the working of artificial lung device, Zierenberg et al. [10] studied the mass transport caused by a pulsating free-stream flow past a circular cylinder. Far from the cylinder, the free stream was represented by superimposing on a steady velocity a (sinusoidal) time-periodic component. The ranges considered for the parameters of interest in the study are: $5 \le \mathrm{Re} \le 40$ and $0.25 \le A \le 0.75$. In almost all investigated cases, a pair of vortices was observed downstream that oscillated in size as well as strength with variations in preceded parameters. Again, Zierenberg et al. [11] fundamentally investigated the blood flow past a circular cylinder (building unit for an artificial lung) filled with an oxygen source taking into consideration the presence of hemoglobin as a distinctive feature of the study. The pulsatile nature in the axially directed blood flow was prescribed with the help of a sinusoidal component of velocity superimposed over the steady velocity, far from the cylinder. The concentration field and flow were

computed for following range of parameters: Re=5-40, $0 \leq A \leq 0.75$ and Womersley parameter (α) = 0.25 & 0.4. Again, the study reports the presence of vortices which oscillated in size as well as strength with variations in A and α. However, for the ranges investigated, varying α did not have any significant influence.

In an attempt to experimentally investigate the non-reversing pulsatile flow around a circular cylinder and its consequent wake structures, making use of the PIV, experiments were performed by Konstantinidis and Balabani [12] in a water rig (recirculating-type) that was developed for generating pulsating flows. The differentiating feature of the study was the independence in controlling the amplitude as well as the pulsation frequencies that were generated as an outcome of blocking part of the flow periodically making use of a rotating slot valve. The amplitude was varied by adjusting the amount of the perturbed and/or unperturbed flow. The study reported measurements keeping Re fixed at 2150. A resonant wake was formed as a consequence of the vortex shedding being locked-on to the pulsation frequency sub-harmonics. The coherent and total Reynolds stress distributions and the mean velocity field went on to highlight the systematic modification of the average wake structures by the pulsating flow. This modification is an outcome of the changes in the vortex formation and shedding dynamics. The following trends were observed as the forcing amplitude grew: (1) decrease in size of the vortex formation region and the recirculation bubble; (2) asymptotic increase in the global peaks of the coherent and total Reynolds stress distribution; and (3) linear increase in the mean drag coefficient as well as the vortex strength. As a result of the increase in the strength of the vortices shed downstream of the formation region, the wake was found to be wider in pulsating flow. Liang and Papadakis [13] analyzed the pulsating cross-flow over a cylinder. For this purpose, the subcritical Re = 2580 was chosen. The estimates were profoundly compared with the very detailed mean velocity and Reynolds stress experiments performed using the PIV technique in a 72 mm $\times$72 mm cross-section duct. The authors examined the instantaneous patterns of flow as well as quantify the effects of external flow pulsation on the flow characteristics, namely the Strouhal number, drag and lift coefficients, formation length of vortex and the vortex strength. Pulsating flow conditions had the following influence: (1) the rms values of the lift as well as the drag coefficients grew notably large; (2) mean drag increased; and (3) the vortex formation length dropped.

Iwai et al. [14] examined the characteristics of heat transfer of a cylindrical bluff body that had been exposed to slow, zero-mean velocity oscillating flow. The authors studied the effects of changing frequency and the flow oscillation amplitude in the range where the flow was bound to remain laminar and where the particle travelled back and forth at distances large enough compared to the diameter of the cylinder. The study measures the space and time averaged Nusselt number and also develops the correlations for Nusselt number in terms Re and *Ri*. It was identified that the heat transfer could be amplified by the motion of local fluid triggered by the vortices around the bluff body, during such period.

Zhao and Cheng [15] numerically simulated oscillations in flow past a pair of circular cylinders placed in two different orientations: side-by-side and tandem arrangements. As a parameter of interest, the influence of gap arrangements (gap ratios, represented by G = 0.5-5; where $G=L/D$, L being the center to center gap between cylinders) and the K_C (that ranged from 1 to 12) over the flow regimes were reported. The results of the flow regimes for the two cylinders system were much in accordance with those observed for a single cylinder system except for the flow pattern, particularly due to the interaction between the cylinders. At sufficiently large gap ratios, the shedding resembled that of a single cylinder case. On the other hand, in case of tandem arrangement, the flow regimes resembled that of a single cylinder at very small gaps. In another study, Tong et al. [16] numerically investigated a flow which sinusoidally oscillated around four cylinders which were ordered in an in-line square arrangement for values of Re ranging from 20 to 200 and K_C from 1 to 12. On the basis of known flow regimes in oscillatory flow around a cylinder, the study identified six reflection symmetry regimes and two spatio-temporal symmetry regimes. At small gap distances in particular, the study went on to establish that the four cylinders acted very similar to a single unit and also that the flow fields resembled to those around a cylinder (having a large effective diameter).

Author(s)	Study	Parameters/Variables
Chandra and Chhabra [1]	Heat transfer due to forced convection from a semi-circular cylinder immersed in unconfined flowing Newtonian fluids	Prandtl number (Pr = 0.72-100) and Reynolds number $(0.01 \le \mathrm{Re} \le 39.5)$
Chandra and Chhabra [2]	Explored the variation of Nusselt number (Nu) along with the drag coefficient (C_D), incorporating power law fluids into the system	$0.01 \le \mathrm{Re} \le 30;\ 0.2 \le n$ (power-law index) ≤ 1.8 and $1 \le \mathrm{Pr} \le 100$
Chandra and Chhabra [3]	Examined the laminar vortex shedding regime for another set of conditions	$40 \le \mathrm{Re} \le 140$; $0.7 \le \mathrm{Pr} \le 50$; and $0.2 \le n \le 1.8$
Kumar and Dhiman [4]	Numerical simulation of incompressible Newtonian forced flow and heat transfer characteristics of a long heated semi-circular obstruction in a confined channel	Re = 1-40; β = 16.67–50%; the working fluid being air
Kumar et al. [5]	For the case of power law fluids, examined forced convection around a confined heated semi-circular cylinder	n = 0.2-1.8; β = 25%; Pr = 50 and Re = 1-40
Qamar et al. [6]	Investigated the flow around an oscillating cylinder in a pulsatile flow environment	$5<\mathrm{Re}<20$; $0.33< K_C <1$; and $0.5D<$cylinder oscillation amplitude$<D$
Al-Sumaily and Thompson [7]	Examined the changes to the heat transfer and flow induced by a steady and sinusoidally varying flow past a cylindrical bluff body for two configurations: (1) cylinder mounted in a horizontal empty channel; and (2) cylinder mounted in a horizontal porous-material filled channel	Re = 1–250 for different types of porous materials keeping the structural properties constant
Lin et al. [8]	Designed an experimental prototype of TAL, that serves as a bridge towards lung transplantation, comprises of cylindrical fibers (hollow) through which the air (rich in oxygen) and the blood (poor in oxygen) flows around	Stokes numbers (N_S) = 0.18-0.37; Re = 1, 3 and 5
Lin et al. [9]	Experimentally studied the pulsatile flow for different geometric arrangements	Re = 1–5 and N_S = 0.17–0.38 across three different cylinder configurations, tandem ($\alpha = 0^\circ$), staggered ($\alpha = 45^\circ$), and

		side-by-side ($\alpha = 90^{\circ}$)
Zierenberg et al. [10]	Studied the mass transport caused by a pulsating free-stream flow past a circular cylinder	$5 \le \mathrm{Re} \le 40$ and $0.25 \le A \le 0.75$.
Zierenberg et al. [11]	Investigated the blood flow past a circular cylinder (building unit for an artificial lung) filled with an oxygen source taking into consideration the presence of hemoglobin as a distinctive feature of the study	Re = 5-40; $0 \le A \le 0.75$ and Womersley parameter (α) = 0.25 & 0.4.
Konstantinidis and Balabani [12]	Experimentally investigated the non-reversing pulsatile flow around a circular cylinder and its consequent wake structures, making use of the PIV in a water rig (recirculating-type) that was developed for generating pulsating flows	Re fixed at 2150
Liang and Papadakis [13]	Analyzed the pulsating cross-flow over a cylinder	Subcritical Re = 2580
Iwai et al. [14]	Examined the characteristics of heat transfer of a cylindrical bluff body that had been exposed to slow, zero-mean velocity oscillating flow	$10 \le A/D \le 38$ and $0.2 \le f \le 1$
Zhao and Cheng [15]	Numerically simulated oscillations in flow past a pair of circular cylinders placed in two different orientations: side-by-side and tandem arrangements	Gap ratios, G = 0.5-5 (where G=L/D, L being the center to center gap between cylinders) and KC = 1 to 12
Tong et al. [16]	Numerically investigated a flow which sinusoidally oscillated around four cylinders which were ordered in an in-line square arrangement	Re = 20-200 and K_C = 1-12

TABLE A. Summary of literature referred

CHAPTER 2. MATHEMATICAL FORMULATION

2.1. Problem statement

Figure 1 provides the schematic diagram of the case considered. The study aims at predicting the flow as well as the heat transfer characteristics from a semi-circular cylinder placed in a long horizontal empty channel (which is effectively two-dimensional since the extent of the channel in the neutral direction is taken to be sufficiently large), under non-zero mean pulsatile flow. It is assumed that the semi-circular cylinder is heated isothermally at a constant temperature (T_w) and is being cooled simultaneously by an incoming flow which is also at a constant temperature (T_∞).

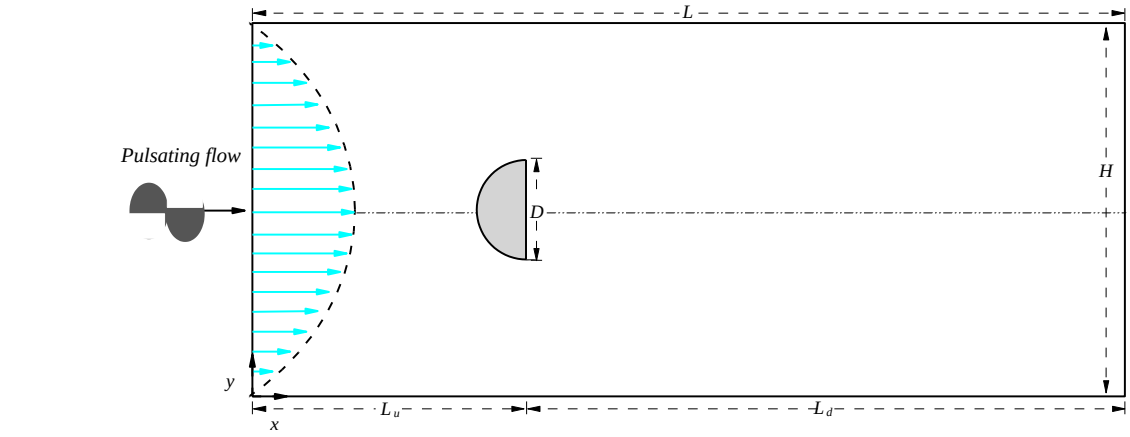

FIGURE 1. Schematic of confined forced-convection pulsatile flow past a semi-circular cylinder mounted in a two-dimensional horizontal empty channel with β = 25%

The geometrical relationships are set as follows: the height and the length of the computational domain are fixed as H and L ($=L_u + L_d$), respectively in lateral and axial dimensions. The semi-circular cylindrical obstruction is mounted at the center-line at an upstream distance equal to L_u from the inlet or at a downstream distance equal to L_d from the outlet. The channel confinement or the blockage ratio is chosen to be D/H = 25% (in concurrence to the relevant confined domain studies such as Kumar et al. [5]; Al-Sumaily

and Thompson [7]; Zdravkovich [17]; Bijjam & Dhiman [18]; Abbassi et al. [19]; Srikanth et al. [20]; Agarwal & Dhiman [21]; and Rasool et al. [22]), *D* being the unit scale length cylinder diameter, and *H* the height of channel. The time period of sinusoidal oscillations τ, while the amplitude is *A*. Two non dimensional parameters, namely the velocity perturbation amplitude (*A*) and the frequency of pulsation (represented by $St = fD/U$, where $f = 1/\tau$ is the forcing frequency) specify the character of the pulsating flow.

In an attempt to minimize any possible variations in the physical properties (namely, viscosity and density) resulting out of alterations in temperature, the temperature difference ($T_w - T_\infty$) between the semi-circular cylinder surface and the streaming fluid is kept sufficiently low (i.e., 2 K). Thus effectively, it was assumed that the streaming liquid thermo physical properties are temperature independent. Another major assumption was to consider the viscous dissipation effects negligible. These two assumptions thus restrict the applicability of the findings to situations where the difference in temperatures is either small or not too significant and for moderate viscosity or shearing levels.

2.2. Governing equations

For the case described, the fluid flowing through the horizontal channel is Newtonian. Also, the flow of fluid was assumed to be laminar and incompressible. It was assumed that forced convection strictly dominated the thermal field of the channels and thus it was convenient to ignore the effects of natural convection. Also, for the phases present, the variation in thermo physical properties were assumed negligible. All these assumptions lead us to the following set of governing equations:

Continuity Equation

$$\frac{\partial U_x}{\partial x} + \frac{\partial U_y}{\partial y} = 0 \text{.....} \text{.....} \text{.....} (1)$$

Momentum Equations

x- Component

$$\frac{\partial U_x}{\partial t} + \frac{\partial U_x U_x}{\partial x} + \frac{\partial U_y U_x}{\partial y} = -\frac{1}{\rho}\frac{\partial p}{\partial x} + \frac{\mu}{\rho}\left(\frac{\partial^2 U_x}{\partial x^2} + \frac{\partial^2 U_x}{\partial y^2}\right) \quad \text{.....(2)}$$

y - Component

$$\frac{\partial U_y}{\partial t} + \frac{\partial U_x U_y}{\partial x} + \frac{\partial U_y U_y}{\partial y} = -\frac{1}{\rho}\frac{\partial p}{\partial y} + \frac{\mu}{\rho}\left(\frac{\partial^2 U_y}{\partial x^2} + \frac{\partial^2 U_y}{\partial y^2}\right) \quad \text{.....(3)}$$

Energy Equation

$$\frac{\partial T}{\partial t} + \frac{\partial U_x T}{\partial x} + \frac{\partial U_y T}{\partial y} = \alpha\left(\frac{\partial^2 T}{\partial x^2} + \frac{\partial^2 T}{\partial y^2}\right) \quad \text{.....(4)}$$

2.3. Boundary conditions

Defining the boundary conditions is one of the major criteria to solve flow problems. In the problem under consideration, the flow is confined and is laminar in nature. The detailed set of boundary conditions and their explanation are as follows:

Inlet *(fully developed flow):*

$$U_x = 1.5U[1-(|1-(2y/H)|)^2][1+A\sin(2\pi f\, t)];\ (0 \le y \le H) \quad \text{.....(5)}$$

$$U_y = 0 \quad \text{.....(6)}$$

$$T = T_\infty \quad \text{.....(7)}$$

Top and Bottom Channel Walls *(adiabatic; no slip condition):*

$$U_x = 0 \quad \text{.....(8)}$$

$$U_y = 0 \quad \text{.....(9)}$$

$$\frac{\partial T}{\partial y} = 0 \quad \text{.....(10)}$$

Semi-Circular Cylinder *(no slip condition):*

$$U_x = 0 \text{.....} \text{.....} (11)$$

$$U_y = 0 \text{.....} \text{.....} (12)$$

$$T = T_w \text{.....} \text{.....} (13)$$

Outlet *(zero diffusion flux; at distance far downstream enough from the semi-circular obstacle):*

$$\frac{\partial U_x}{\partial x} = 0 \text{.....} \text{.....} (14)$$

$$\frac{\partial U_y}{\partial x} = 0 \text{.....} \text{.....} (15)$$

$$\frac{\partial T}{\partial x} = 0 \text{.....} (16)$$

CHAPTER 3. NUMERICAL METHOD OF SOLUTION

3.1. Numerical computations

The computations were carried out for the primitive variables (namely, temperature (T) and pressure (p) fields; velocity U_x and U_y) by solving the boundary conditions along with the governing equations. In order to solve the case of incompressible flow, two-dimensional laminar segregated commercial CFD solver Ansys Fluent was employed on the collocated non-uniform grid. User defined functions (UDF) in form of simple C++ code were used to incorporate a completely developed pulsating velocity profile at the inlet of the channel (Section 2.3). A sample UDF has been attached in the Appendix for reference. The method brings into use the QUICK scheme in order to discretize the convective terms. The SIMPLE scheme was employed to solve the pressure–velocity decoupling. The system of algebraic equations was solved bringing into use the Gauss–Siedel iterative method along with the algebraic multi-grid method solver. In the steady regime, the prescribed absolute convergence criteria for the continuity as well as the x- and y- components of the velocity were fixed at 10^{-10} while that for energy this criterion was set at10^{-12}. However, in the unsteady regime these absolute convergence criteria were fixed at 10^{-12} for all.

A Gambit generated computational grid served the purpose of mesh (Figure 2). The zoomed view of the grid has been shown in Figure 2, details of which are as follows: the count of semi-circular cylinder control volumes equals 340 (in accordance with Kumar & Dhiman [4] and Kumar et al. [5]); the grid is very fine with cell size equal to 0.01D clustered around the semi-circular obstacle as well as in the vicinity of channel walls.; however, the largest size of grid (= 0.5D) has been incorporated away from these.

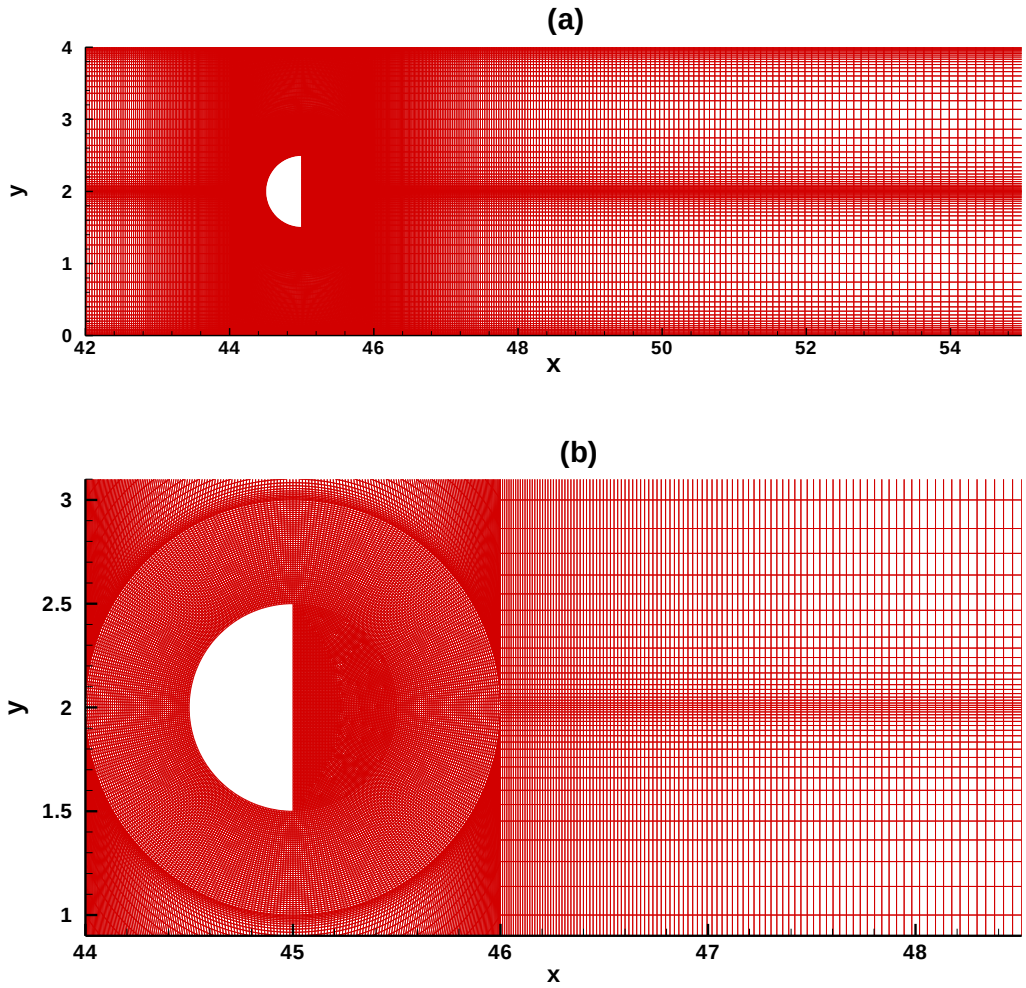

FIGURE 2. Magnified view(s) of the grid around a semi-circular cylinder for β = 25%

3.2. Resolution studies

Resolution studies make sure that the numerically obtained results do not depend on the domain size as well as the grid resolution (spatial) and the time step. These studies have been undertaken here for a single semi-circular cylinder mounted in a long and horizontal channel, the configuration for which has been described in Figure 1. As indicators of convergence, *Nu* and C_D values were monitored in these studies.

3.2.1. Domain size study

The analysis of appropriate domain size is carried out in order to analyze the effects of upstream distances (Table 1) as well as downstream distances (Table 2) on the dimensionless output parameters. Six different domains were examined for this purpose. The computations were carried out to study the influence of the upstream distance on the values of C_D and Nu for L_u = 35D, 45D and 55D at Re = 10 and Pr = 7 for A = 0, 0.1 & 0.6 and St = 0, 0.1 & 2 (Table 1). The percent changes in the values of dimensionless outputs for L_u/D = 45 with respect to L_u/D = 55 were identified to be less than 0.2% for both C_D and Nu. Thus with an aim to keep the present results free from end effects, an upstream distance of L_u/D = 45 is used in this study. On similar grounds, computations were carried out to explore the effects of the downstream distance on the C_D and Nu values for L_d = 110D, 120D and 130D at Re = 100 and Pr = 7 for same set of values of A and St (Table 2). The relative differences were identified to be less than 0.7% for both C_D and Nu for L_d/D = 120 with respect to L_d/D = 130. Therefore the downstream distance of the semi-circular cylinder from the exit plane is taken as L_d/D = 120.

Re = 10; Pr = 7 ($\frac{L_d}{D}=120$)		$\frac{L_u}{D}=35$		$\frac{L_u}{D}=45$		$\frac{L_u}{D}=55$	
A	***St***	***C_D***	***Nu***	***C_D***	***Nu***	***C_D***	***Nu***
-	0	7.9340	5.2171	7.9223	5.2175	7.9223	5.2175
0.1	0.1	7.9456	5.2191	7.9312	5.2189	7.9308	5.2188
0.1	2	7.9373	5.2178	7.9234	5.2179	7.9233	5.2180
0.6	0.1	8.3146	5.2579	8.3091	5.2480	8.2921	5.2560
0.6	2	8.0342	5.2473	8.0154	5.2523	8.0114	5.2472

TABLE 1. Effect of upstream distance on the dimensionless output parameters for Re=10 and Pr=7 at different values of A and St

Re = 100; Pr = 7 ($\frac{L_u}{D}=45$)		$\frac{L_d}{D}=110$		$\frac{L_d}{D}=120$		$\frac{L_d}{D}=130$	
A	***St***	C_D	***Nu***	C_D	***Nu***	C_D	***Nu***
-	0	4.2402	18.0290	4.2410	18.0281	4.2410	18.0280
0.1	0.1	4.2319	18.0263	4.2301	18.0389	4.2327	18.0243
0.1	2	4.2617	18.0918	4.2564	18.0893	4.2768	18.0884
0.6	0.1	4.2536	17.4416	4.2595	17.4355	4.2590	17.4309
0.6	2	4.7607	19.6577	4.8011	19.6450	4.7893	19.6491

TABLE 2. Effect of downstream distance on the dimensionless output parameters for Re=100 and Pr=7 at different values of *A* and *St*

3.2.2. Grid resolution study

Grid resolution studies are performed with a motive to identify the spectral resolution that ensures high accuracy at the cost of least computational expense. This involves identifying the number of control volumes and the δ/D ratio at which the solution becomes grid independent. For this purpose, three structures of the grid (represented symbolically as G1, G2 and G3 with respectively 250, 340 and 400 control volumes present at the surfaces of the semi-circular cylinder) were chosen and the effects were administered in terms of dimensionless output parameters C_D and *Nu* for Re = 100, Pr = 7, β = 25%, *A* = 0.1, 0.6 and *St* = 0, 0.1, 2 (Table 3). The relative difference in C_D values for G2 (340 CVs) with respect to those for the finest of all grid considered, i.e. G1 (400 CVs), was lesser than 1.6%. Also considering the *Nu* values, this relative difference in values for G2 (340 CVs) with respect to those for G1 (400 CVs) was identified to be lesser than 0.8%. Therefore as a final choice, grid G2 was considered apt for generating further results.

Re = 100; Pr = 7		$\frac{L_u}{D}=45;\ \frac{L_d}{D}=120$					
		G1		**G2**		**G3**	
δ/D		0.008		0.01		0.02	
CVs on Semi-Circular Cylinder		400		340		250	
Total Number of Cells in Domain		117323		101042		79970	
A	***St***	C_D	***Nu***	C_D	***Nu***	C_D	***Nu***
-	0	4.1727	18.1760	4.2410	18.0281	4.3340	18.1369
0.1	0.1	4.1650	18.1643	4.2301	18.0389	4.3293	18.1156
0.1	2	4.1956	18.2363	4.2564	18.0893	4.3501	18.2143
0.6	0.1	4.2442	17.5251	4.2595	17.4355	4.3032	17.3913
0.6	2	4.7643	19.7680	4.8011	19.6450	4.9085	20.1278

TABLE 3. Grid dependence study for Re=100 and Pr=7 at different values of *A* and *St*

3.2.3. Time step study

Tabulated here in Table 4 are the C_D and *Nu* values obtained with two different time steps, $\Delta t = 0.001$ and $\Delta t = 0.005$ for Pr = 7 at maximum value of the Re considered in the study i.e. Re = 100. The C_D and *Nu* values obtained for both the time steps are appreciably in agreement to one another. Therefore as a final choice, the non-dimensional value of $\Delta t = 0.001$ is taken into consideration in the following study.

Re = 100; Pr = 7		$\frac{L_u}{D}=45;\frac{L_d}{D}=120$			
		$\Delta t=0.001$		$\Delta t=0.0005$	
A	***St***	C_D	***Nu***	C_D	***Nu***
-	0	4.2410	18.0281	4.2992	18.1903
0.1	2	4.2564	18.0893	4.3092	18.2607
0.6	2	4.8011	19.6450	4.8982	20.0015

TABLE 4. Influence of time step (Δt) for Re = 100 and Pr=7 at different *A* and *St*

CHAPTER 4. RESULTS & DISCUSSION

Discussed here are the findings of forced convection from a confined semi-circular cylinder mounted horizontally in a pulsating flow environment. The study serves the purpose of examining the influence of pulsating flow variables *A* and *St* over the heat transfer. In an attempt to cover the range of parameter values that have been previously examined in the literature (Al-Sumaily and Thompson [7]) for a circular cylinder, the present research has been undertaken for the following set of parameter values: $10 \le \mathrm{Re} \le 100$; $0 \le St \le 2$; $0 \le A \le 0.6$ and Pr=7.

As per the knowledge of the authors, there exists no literature concerning the flow of pulsating fluids past a semi-circular cylindrical obstacle mounted in a confined horizontal domain. Thus the benchmarking of the present procedure (to obtain numerical solution) was done for the case of a complete cylinder placed in a similar wall confinement of 25% for Re=10, 40 and 100 and Pr=7 at different values of *A* and *St*. The conditions as well as the computational domain were identical to that of Al-Sumaily and Thompson [7]. Excellent agreement was observed between the results generated in the present study and the values plotted in the literature (Table 5).

A	***St***	***Nu*** (Present Work)			***Nu*** (Al-Sumaily & Thompson [7])		
		Re = 10	Re = 40	Re = 100	Re = 10	Re = 40	Re = 100
0.1	1	5.1506	9.2438	15.2171	5.1632	9.2489	15.2444
0.1	2	5.1512	9.2312	15.2078	5.1640	9.2418	15.2444
0.3	1	5.1459	9.3371	15.3003	5.1526	9.3129	15.3222
0.3	2	5.1489	9.2486	15.2688	5.1588	9.2418	15.2999
0.6	1	5.1194	9.6173	15.6661	5.1202	9.5476	15.7999
0.6	2	5.1388	9.3222	15.4564	5.1447	9.2418	15.3444

TABLE 5. Comparison of Nusselt number results for pulsating flow around a circular cylinder with literature (Al-Sumaily & Thompson [7]) at various values of Re, *A* and *St* in the confined domain

4.1. Nature of fluid flow

Nature of the fluid flow has been presented in Table 6 as steady and/or (periodic) unsteady flow regimes for the entire range of settings covered. The unsteadiness is confirmed by the outcomes of the time dependent calculations that were performed in the full computational domain. For higher Re values ($\mathrm{Re} \geq 50$), unsteady (periodic) flow is observed over the complete range of *A* and *St* considered. However as expected, at smaller Re values (Re < 50), steady flow regimes were observed for *St* = 0. The flow is again identified to be (periodic) unsteady at these Re values for *St* > 0.

Re	***A***	***St***			
		0	0.1	1	2
10	0.1	s	us	us	us
	0.6	s	us	us	us
25	0.1	s	us	us	us
	0.6	s	us	us	us
50	0.1	us	us	us	us
	0.6	us	us	us	us
75	0.1	us	us	us	us
	0.6	us	us	us	us
100	0.1	us	us	us	us
	0.6	us	us	us	us
s = steady state; us = unsteady state					

TABLE 6. Identification of nature of fluid flow patterns: steady and unsteady flow regimes

4.2. Flow and thermal patterns

The flow (streamlines) as well as the thermal patterns (isotherm contours) in the vicinity of the semi-circular cylinder were investigated for the considered range of parameters. Figures 3-7 show the streamline contours for all Re considered excluding the case of $St = 0$. Figure 8 shows these contours at $St = 0$ for all Re. For Re = 10 and 25 i.e. in the steady regime (Figures 3 and 4), two standing symmetric vortices were observed that rotated in directions opposite to one another behind the semi-circular obstacle (except for the case when $A = 0.1$ and $St = 2$ for Re = 10). As expected, with rise in Re (from 10 to 25) for a given pair of A and St, the size of these vortices increased. For $\mathrm{Re} \geq 50$, instantaneous streamlines (Figures 5-7) were generated. Periodic unsteady cylinder wakes are observed at all frequencies (i.e. St) considered.

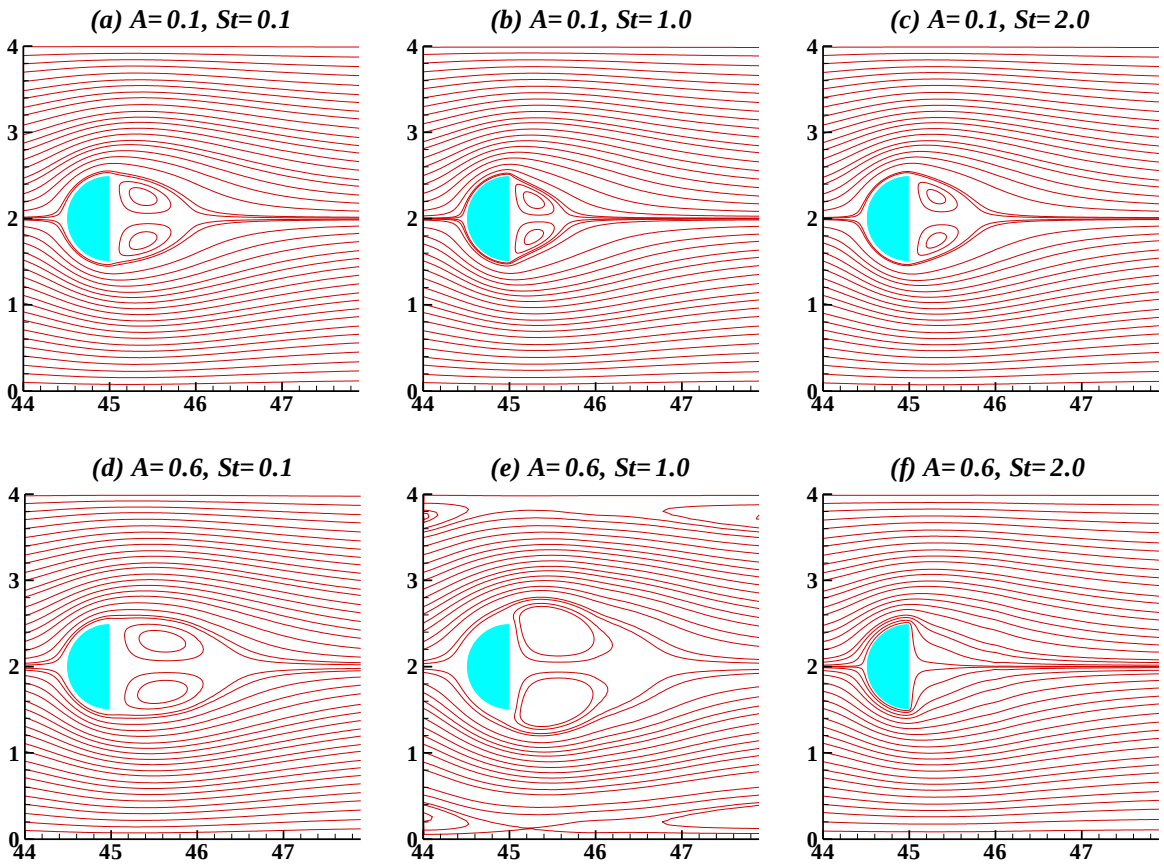

FIGURE 3. Streamlines at Re = 10 for A = 0.1, 0.6 and St = 0.1, 1, 2

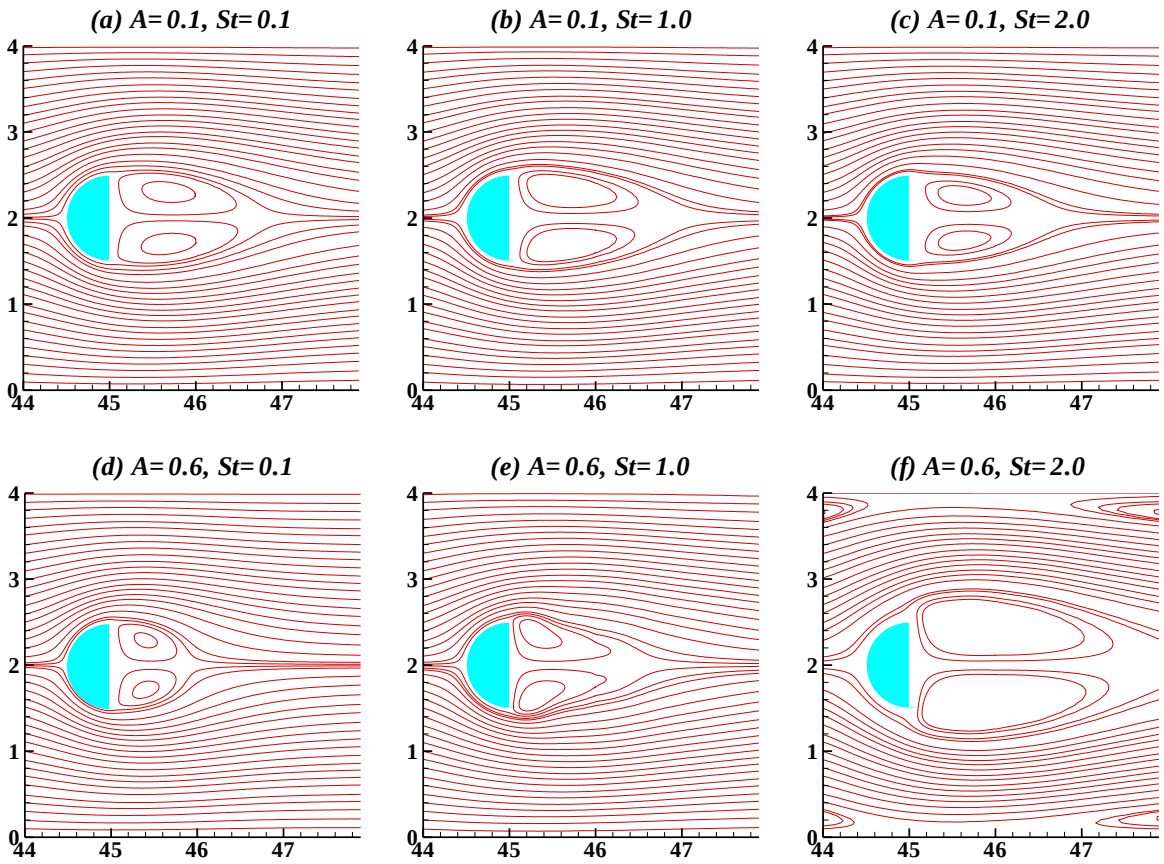

FIGURE 4. Streamlines at Re = 25 for A = 0.1, 0.6 and St = 0.1, 1, 2

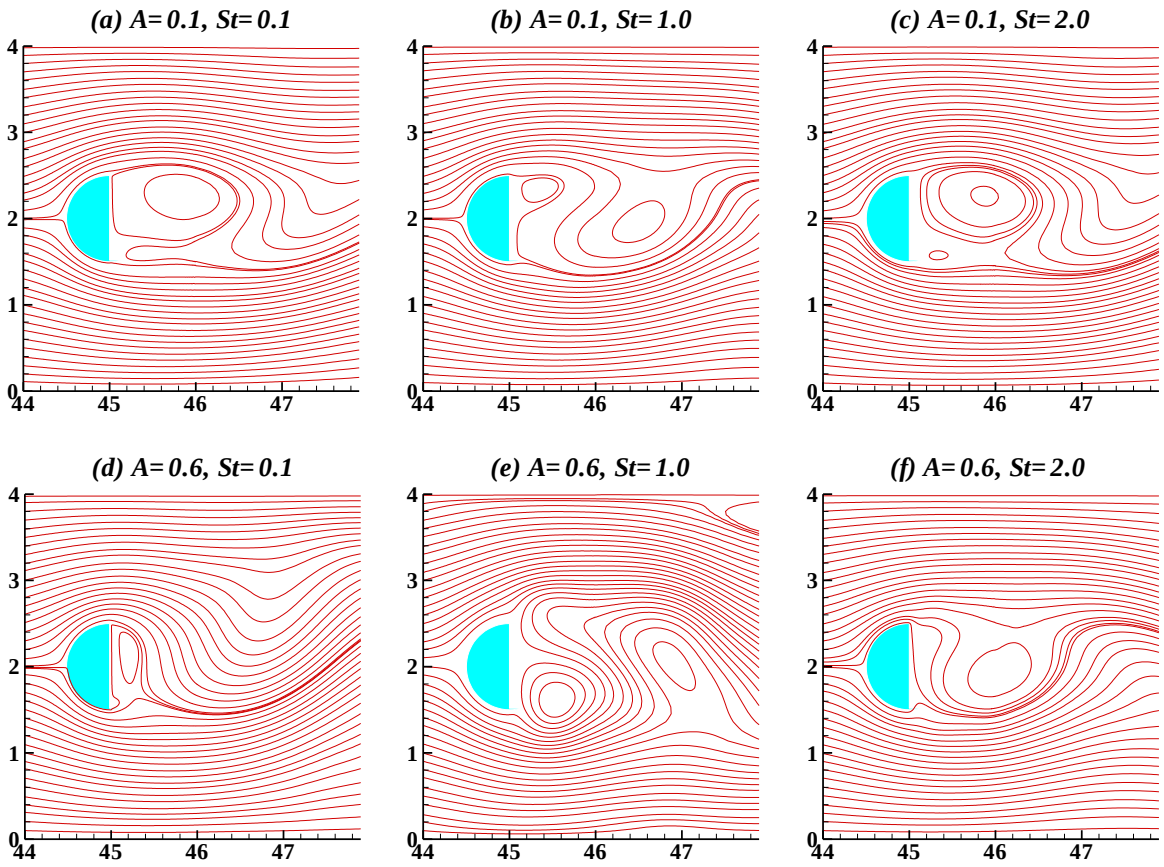

FIGURE 5. Instantaneous streamlines at Re = 50 for A = 0.1, 0.6 and St = 0.1, 1, 2

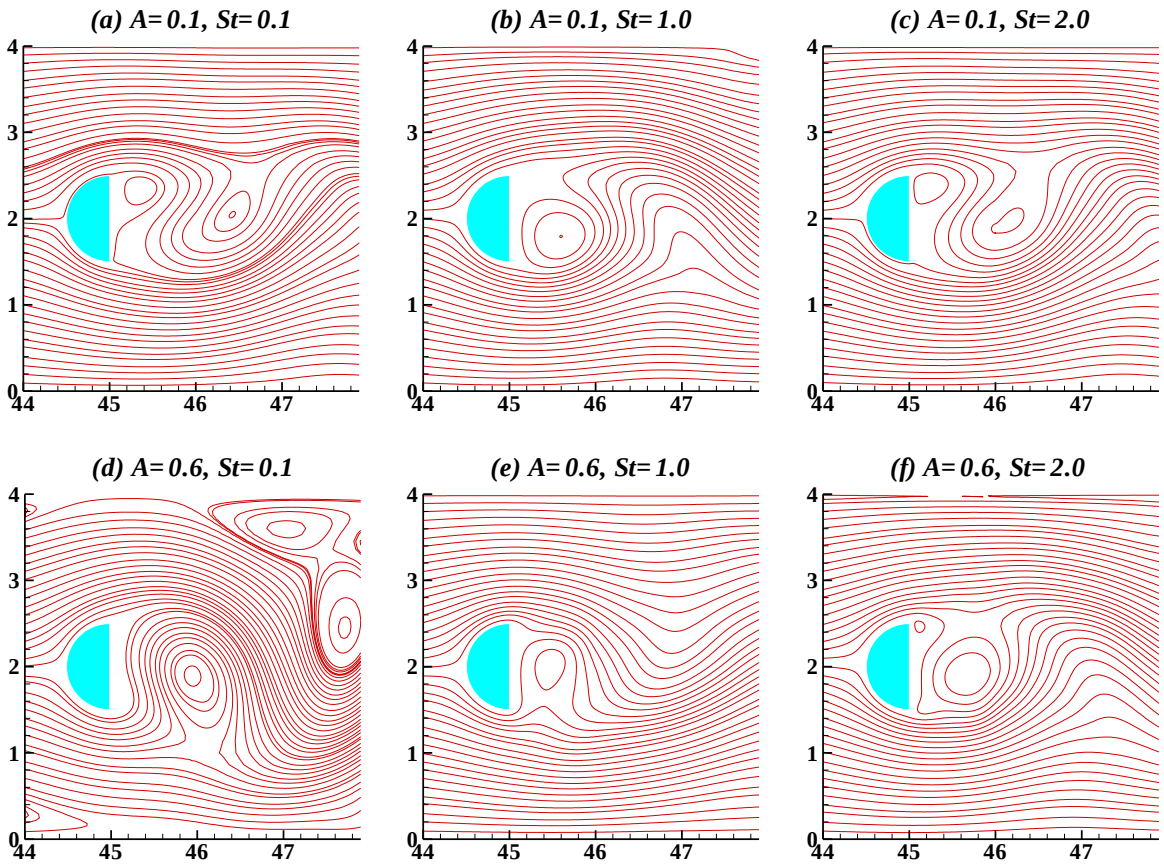

FIGURE 6. Instantaneous streamlines at Re = 75 for A = 0.1, 0.6 and St = 0.1, 1, 2

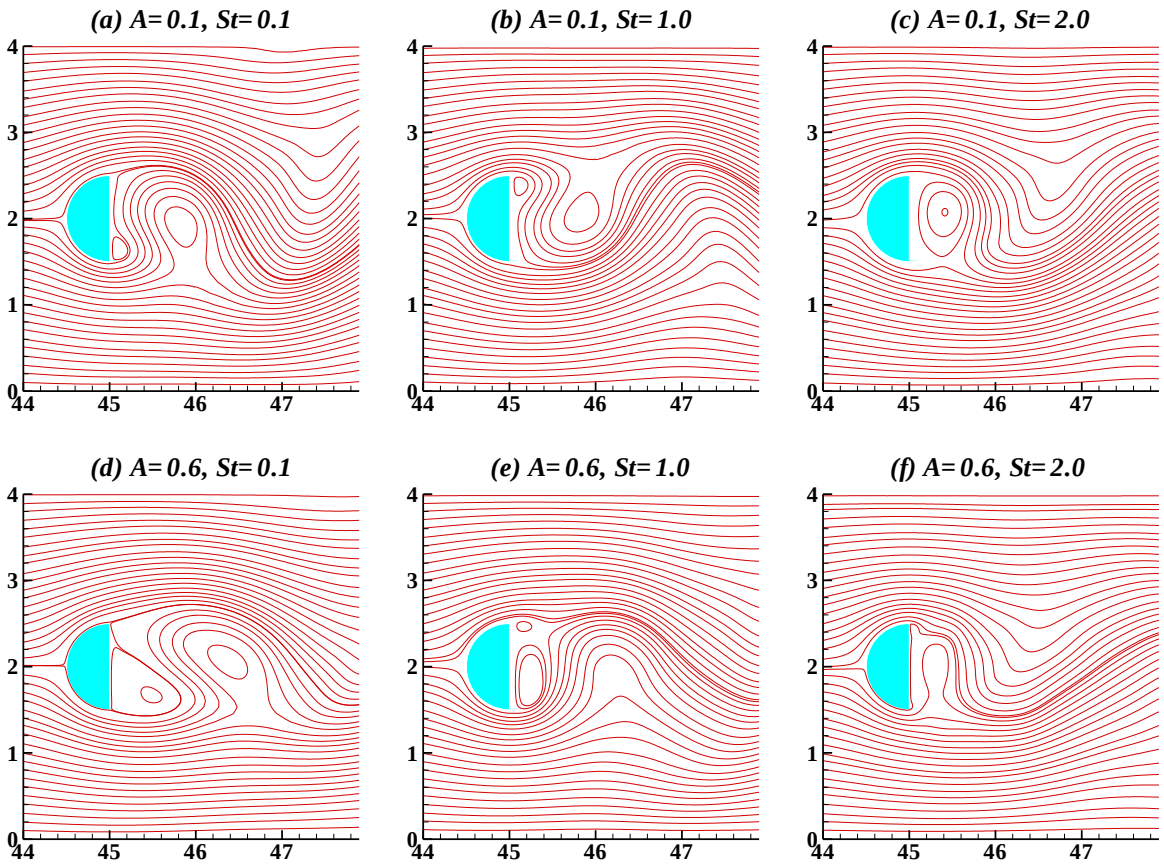

FIGURE 7. Instantaneous streamlines at Re = 100 for *A* = 0.1, 0.6 and *St* = 0.1, 1, 2

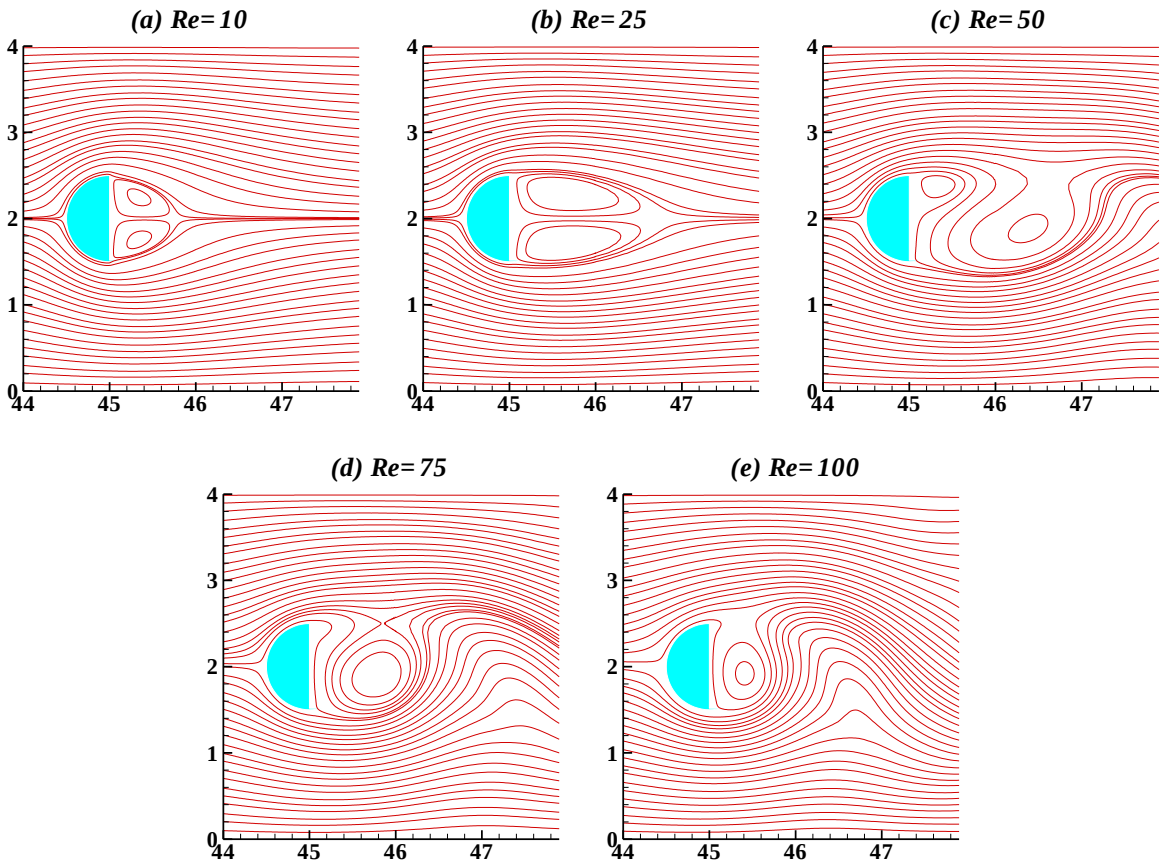

FIGURE 8. Streamlines for *St* = 0 at different Re

When fluid flows over a bluff body, typical separation occurs between the boundary layer and the surface. This separation might occur at any sharp corner or near the maximum width of the body. Shear layers are formed on both sides of the body due to the separated flow. A velocity gradient exists across these shear layers because of the fact that the outer portion of each shear layer that is in contact with the free stream moves faster than its inner portion which was in contact with the surface of the body. Thus the shear layer is rolled up and two opposite rotating vortices are formed behind the body. Vortices are shed into the stream because of the tendency of the opposing shear layer to be drawn downstream due to the circulation in shear layer. Natural disturbances associated with flow can however make the shear layers unstable and can also trigger one of these vortices (among the pair) to grow faster and bigger than the other. The growth in the larger vortex is so much that it draws the opposite shear layer across the near wake. Consequently, the body releases this vortex which is then convected downstream in the wake. Now in turn, the (other) vortex on the opposite side grows faster in the absence of the first vortex and this time the shear layer on the first side rolls up forming a new vortex. The process continues in this way leading to the formation of a 'street' of vortices that appear in the wake of the body. Downstream, at large distances from the body, these vortices (in the wake) diffuse and fade out eventually as they coalesce into one another.

Figures 9-13 show the thermal contours for all Re considered excluding the case of $St = 0$. Figure 14 shows these contours at $St = 0$ for all Re. Temperature street is formed behind the semi-circular cylindrical obstacle. As per the expectations, the maximum clustering of isotherms was observed at the upstream (curved) surface of the semi-circular cylinder while the downstream (flat) surface had the minimum amount of clustering. This leads us to realize that high heat transfer rate exists at the curved surface in comparison to the flat one. In concurrence to the findings of Kumar et al. [5], Dhiman [23] and Bharti et al. [24] an increase in the temperature gradient (also a consequent increase in the rate of heat transfer) was observed around the obstacle as Re grew. This is explained by the increase in large amount of fluid circulation eventually leading to the thinning of thermal and momentum boundary layers. In general, the trends of heat transfer rate observed here displayed strong dependence on the values of *Re*.

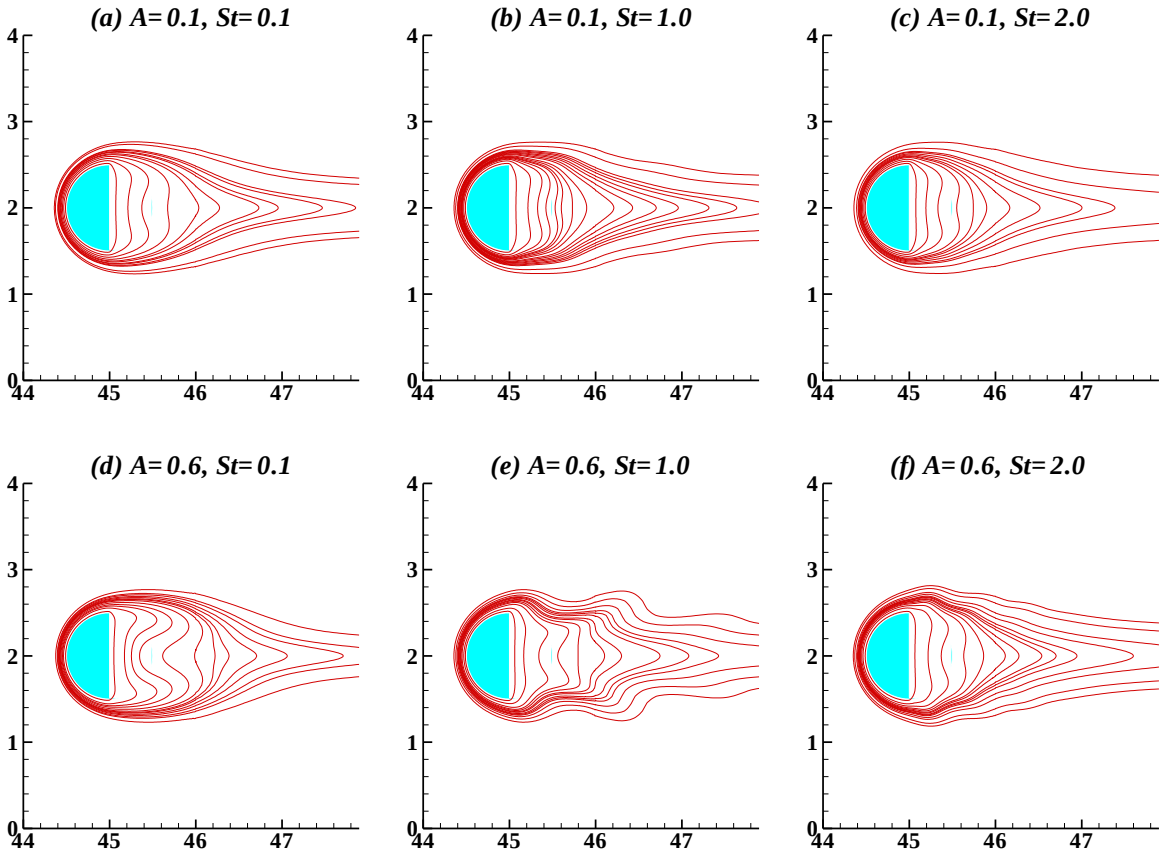

FIGURE 9. Isotherm contours at Re = 10 for A = 0.1, 0.6 and St = 0.1, 1, 2

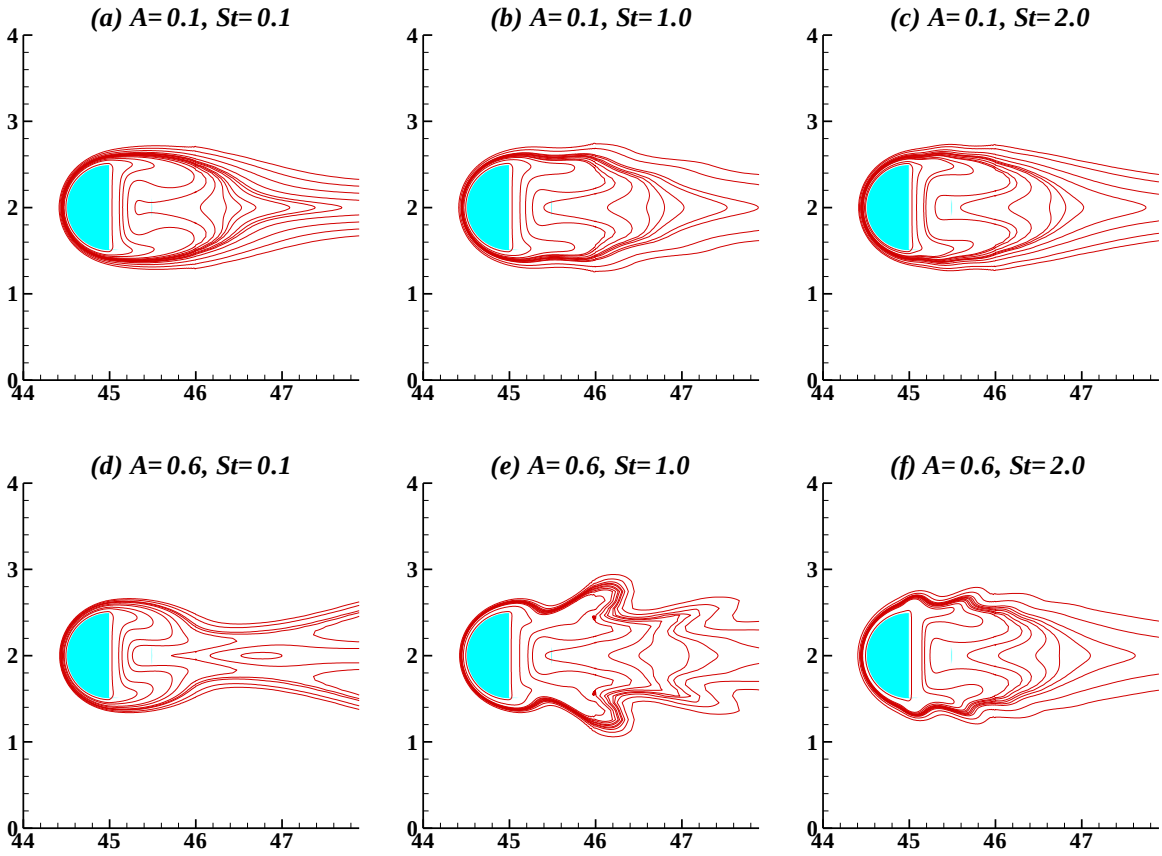

FIGURE 10. Isotherm contours at Re = 25 for A = 0.1, 0.6 and St = 0.1, 1, 2

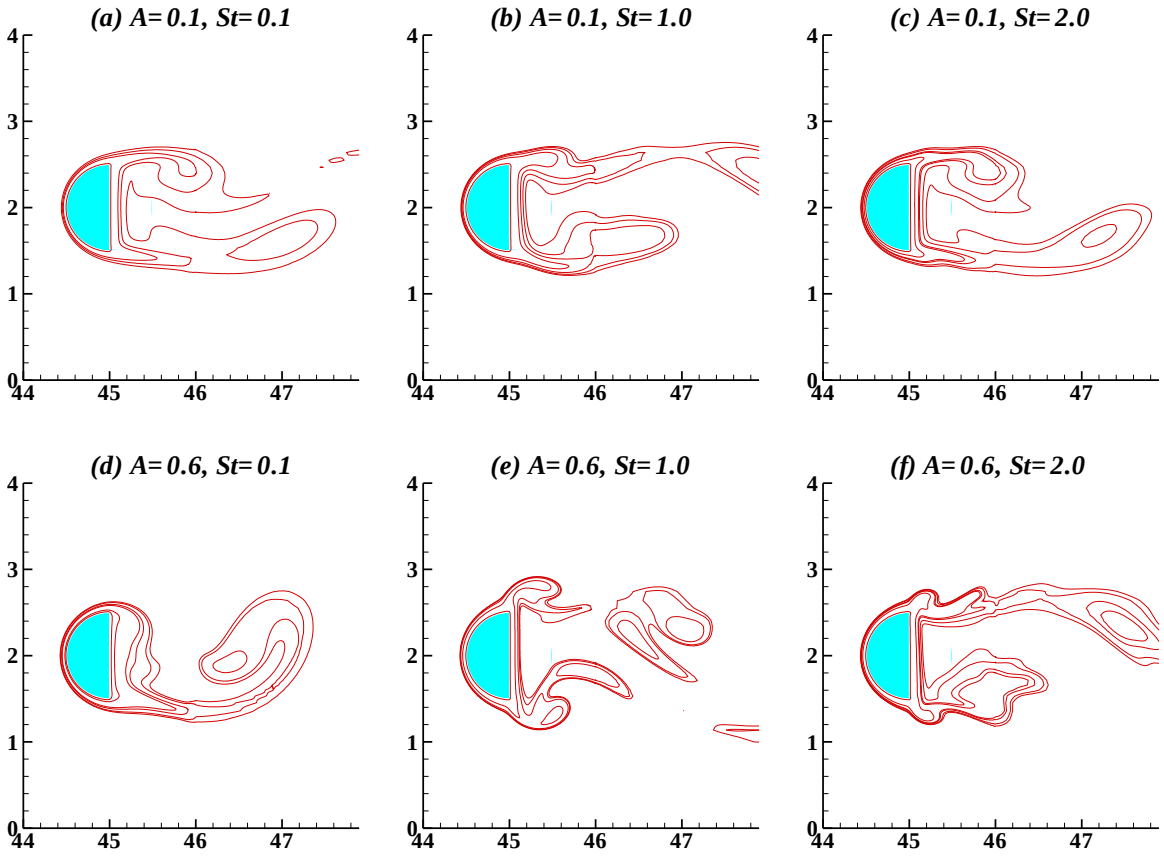

FIGURE 11. Instantaneous isotherm contours at Re = 50 for A = 0.1, 0.6 and St = 0.1, 1, 2

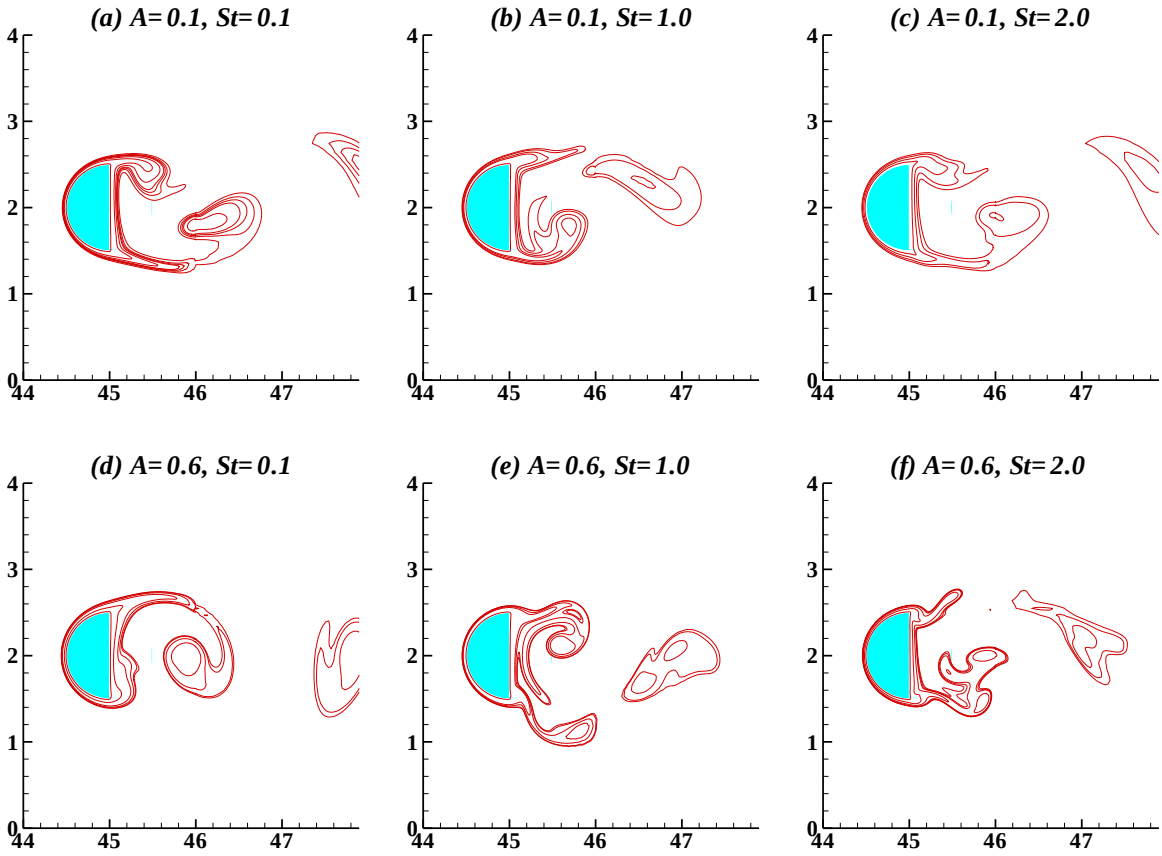

FIGURE 12. Instantaneous isotherm contours at Re = 75 for A = 0.1, 0.6 and St = 0.1, 1, 2

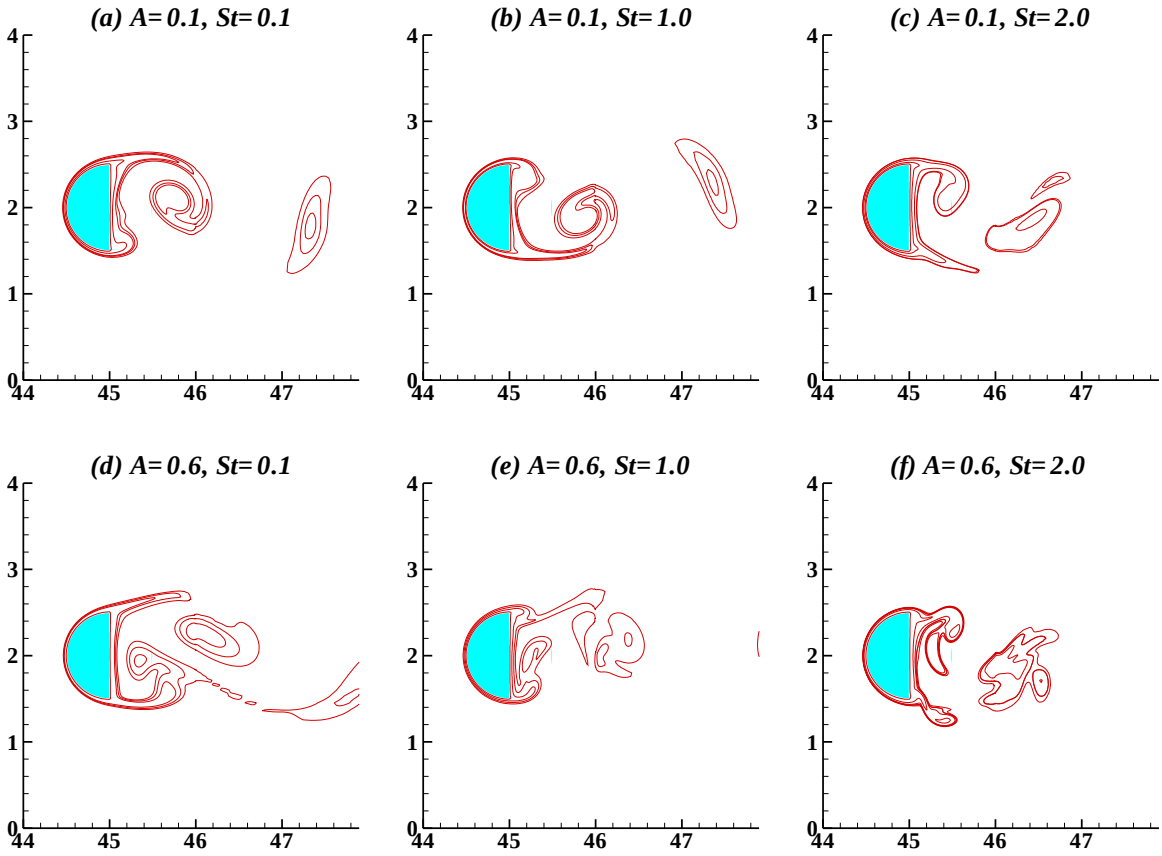

FIGURE 13. Instantaneous isotherm contours at Re = 100 for A = 0.1, 0.6 and St = 0.1, 1, 2

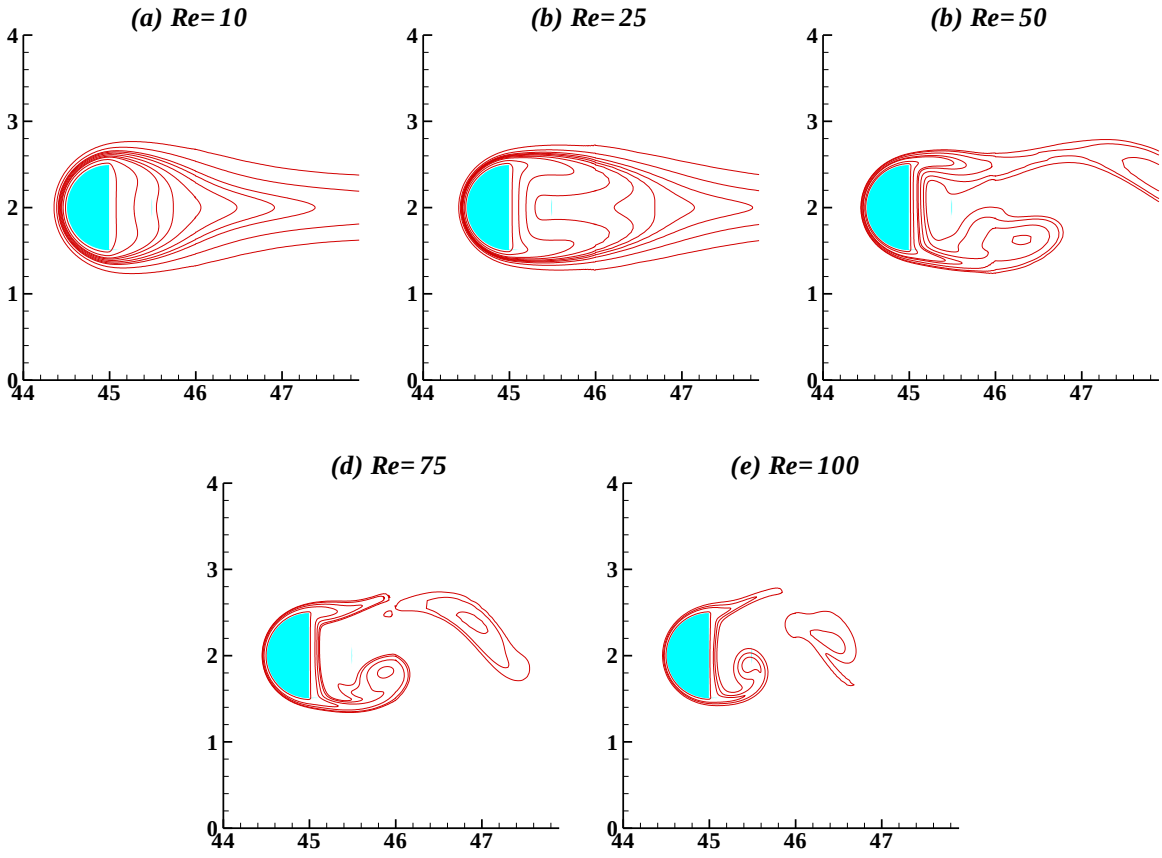

FIGURE 14. Isotherm contours for *St* = 0 at different Re

4.3. Time history of *Nu* and C_D

Figures 15(a-j) reveal the variations (temporal) of the coefficient of drag and the Nusselt number for the considered range of the Re (= 10 to 100) at *St*=0. Plotted here are the instantaneously calculated *Nu* and C_D values against the time step. It was observed that at initial times, the instantaneous values of both *Nu* and C_D fluctuated heavily but later stabilized with time for all the considered cases. As expected for low Re (≤ 25), the *Nu* and C_D values displayed a constant value trend after this stabilization. This justified earlier in this section (nature of fluid flow) that at smaller Re values ($\mathrm{Re} \leq 25$), steady flow regimes were observed for *St* = 0. However for $\mathrm{Re} \geq 50$, both Nu and C_D values individually oscillated between a fixed set of values (varied sinusoidally) after stabilization with time. Additionally, Figures 15(f-j) indicate the trends in growth of *Nu* as Re increases. Similarly, for other sets of values of *St* and *A*, Figures 16-21 reveal the variations (temporal) of the coefficient of drag and the Nusselt number.

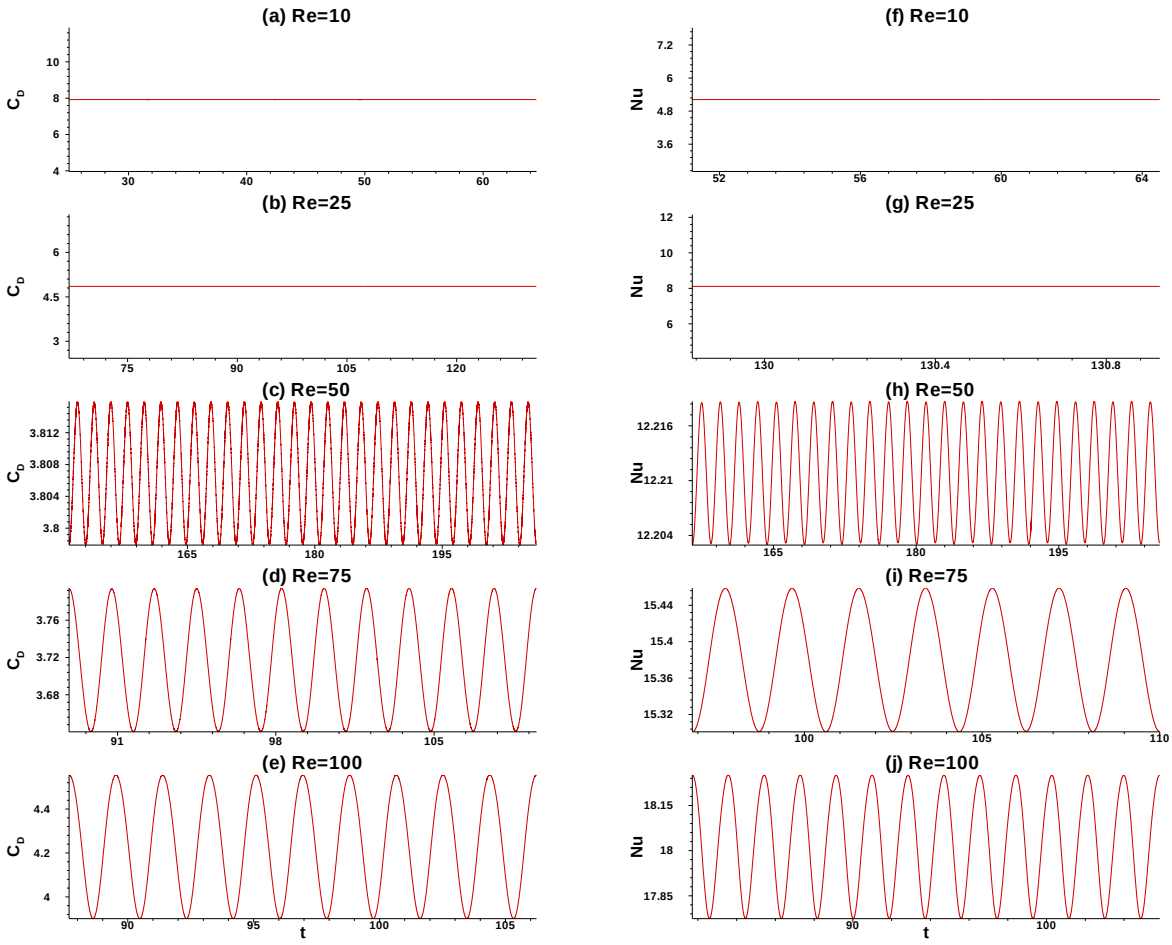

FIGURE 15. Time history of coefficient of drag (a-e) and Nusselt number (f-j) at *St* = 0 for Re = 10, 25, 50, 75, 100 and Pr=7

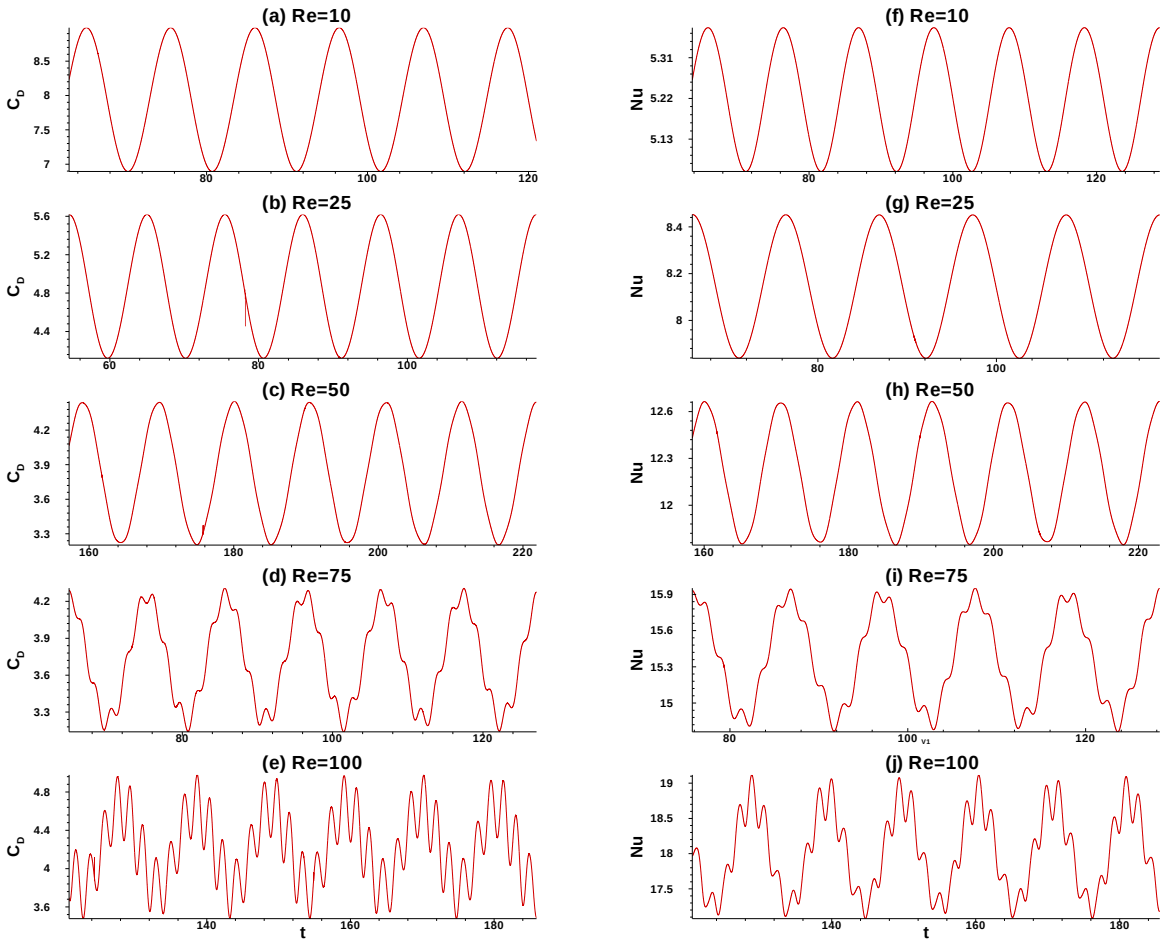

FIGURE 16. Time history of coefficient of drag (a-e) and Nusselt number (f-j) at St = 0.1 & A = 0.1 for Re = 10, 25, 50, 75, 100 and Pr=7

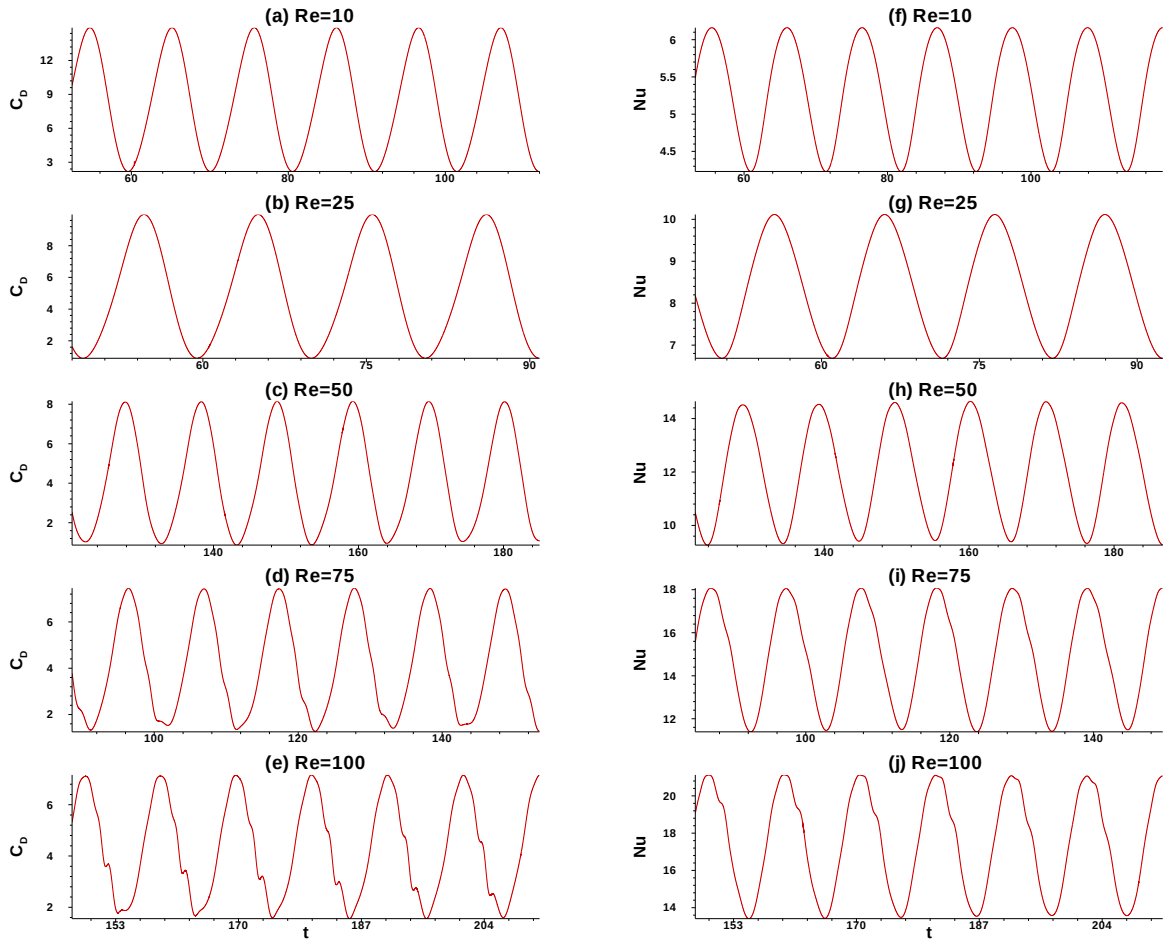

FIGURE 17. Time history of coefficient of drag (a-e) and Nusselt number (f-j) at St = 0.1 & A = 0.6 for Re = 10, 25, 50, 75, 100 and Pr=7

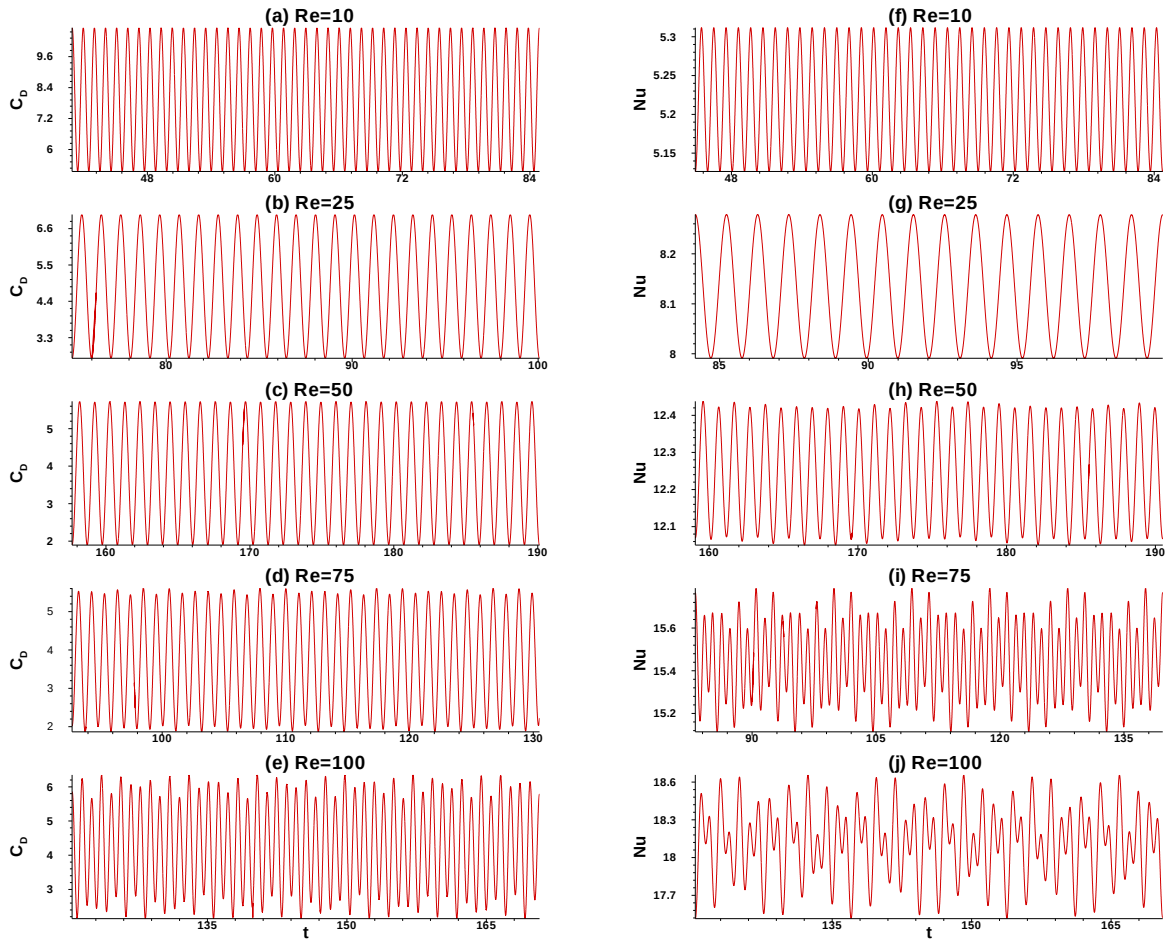

FIGURE 18. Time history of coefficient of drag (a-e) and Nusselt number (f-j) at *St* = 1 & *A* = 0.1 for Re = 10, 25, 50, 75, 100 and Pr=7

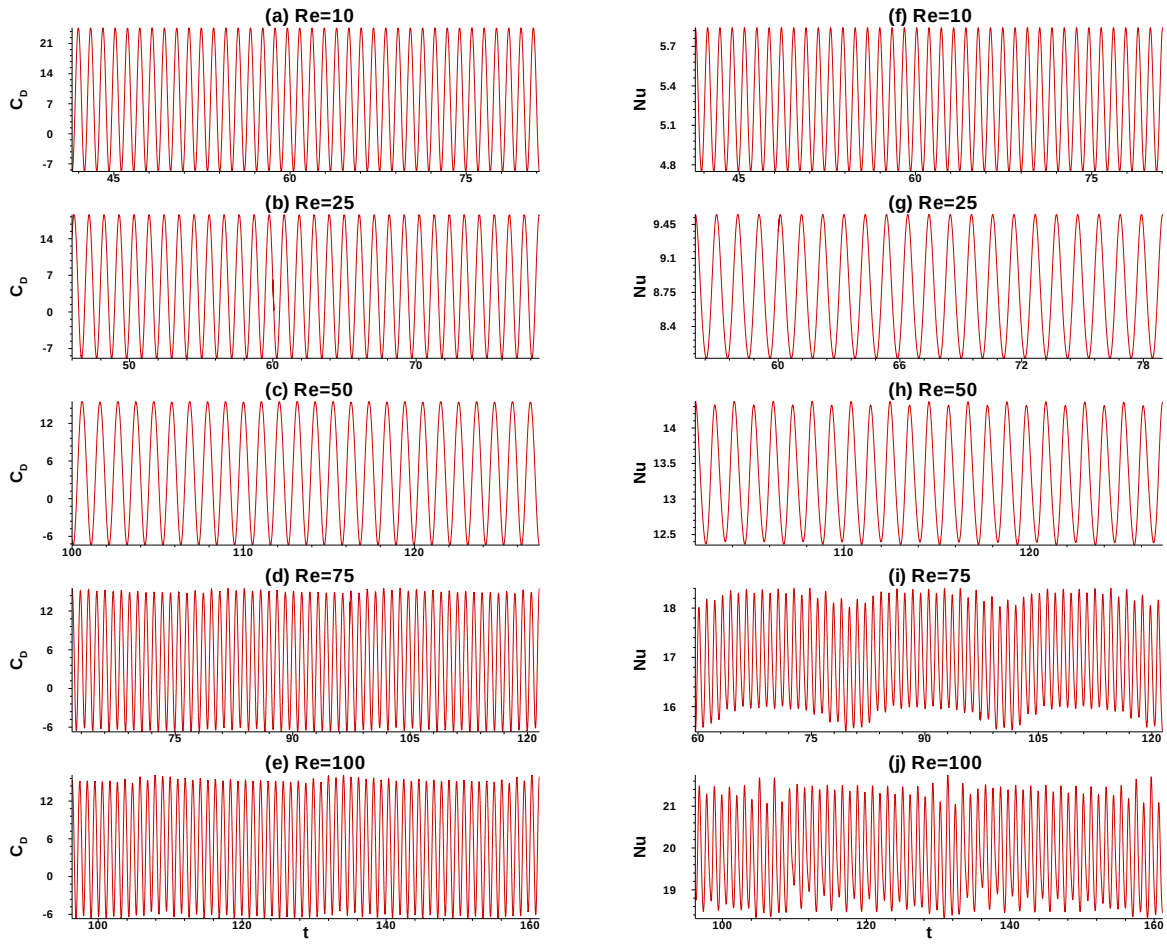

FIGURE 19. Time history of coefficient of drag (a-e) and Nusselt number (f-j) at *St* = 1 & *A* = 0.6 for Re = 10, 25, 50, 75, 100 and Pr=7

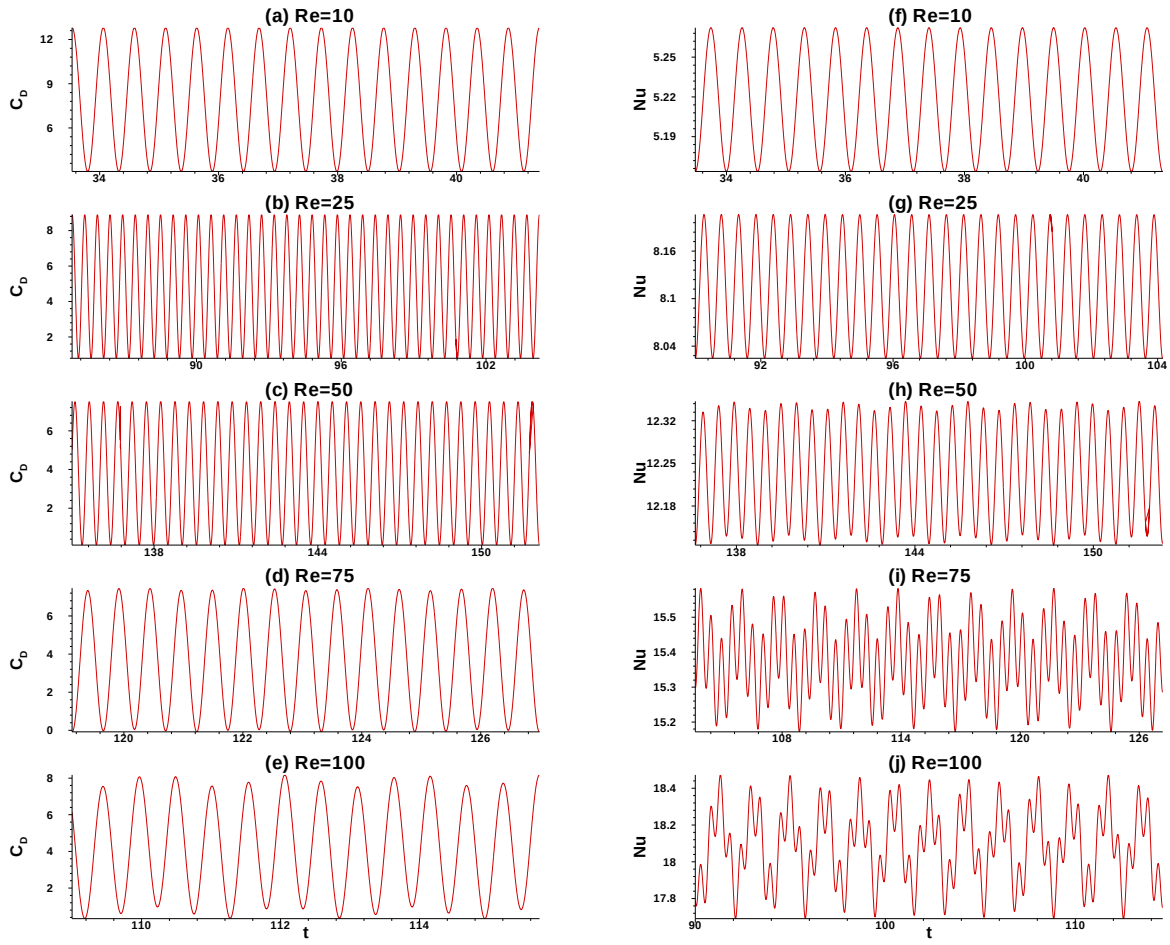

FIGURE 20. Time history of coefficient of drag (a-e) and Nusselt number (f-j) at *St* = 2 & *A* = 0.1 for Re = 10, 25, 50, 75, 100 and Pr=7

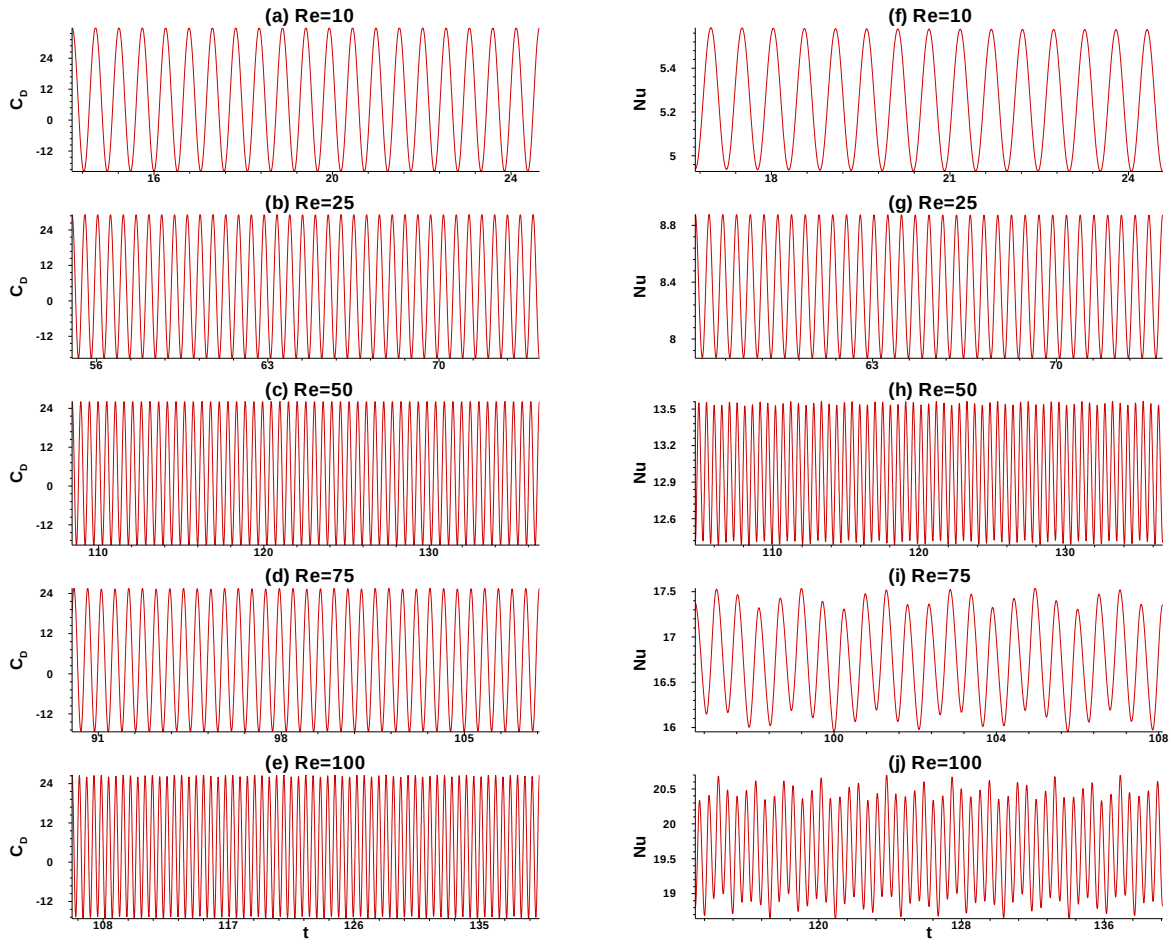

FIGURE 21. Time history of coefficient of drag (a-e) and Nusselt number (f-j) at *St* = 2 & *A* = 0.6 for Re = 10, 25, 50, 75, 100 and Pr=7

4.4. Overall drag coefficient

Drag coefficient (C_D) generally characterizes the force coefficient induced by flow. For a semi-circular cylinder, Figure 22 reveals the trends in which the overall drag coefficient depended upon Re (10, 25, 50, 75 and 100), *St* (0, 0.1, 1 and 2) and *A* (0.1 and 0.6). A complex dependence is displayed by the variation of the coefficient of the total drag on the control parameters Re, *St* and *A*. For all pairs of Re and *St* (excluding *St* = 0), C_D at $A = 0.6$ is larger than C_D at $A = 0.1$. It can be observed for all pairs of *A* and *St* (excluding *St* = 0) that as Re grows up to 75, C_D values decrease. However, the values thereafter increase as Re grows to 100. For all Re considered, the effect of *A* over C_D considerably vanishes at lower *St* for semi-circular cylinder. For the considered ranges of parameters that overlap between the present study and the one conducted by Kumar et al. [5], the values of C_D follow similar trends with Re for *St* = 0. For $\mathrm{Re} \leq 75$, the values of C_D first grew and then fell as *St* increased for high amplitude ($A = 0.6$) values. However for Re = 100, the C_D values grew monotonically with *St* at this amplitude. In fact, for $\mathrm{Re} \leq 25$, the plots of C_D had distinct peaks (maxima). At higher values of *St*, the difference in C_D values for $A = 0.1$ and 0.6 grew with increase in Re. A maximum of around 22% augmentation in coefficient of drag is obtained.

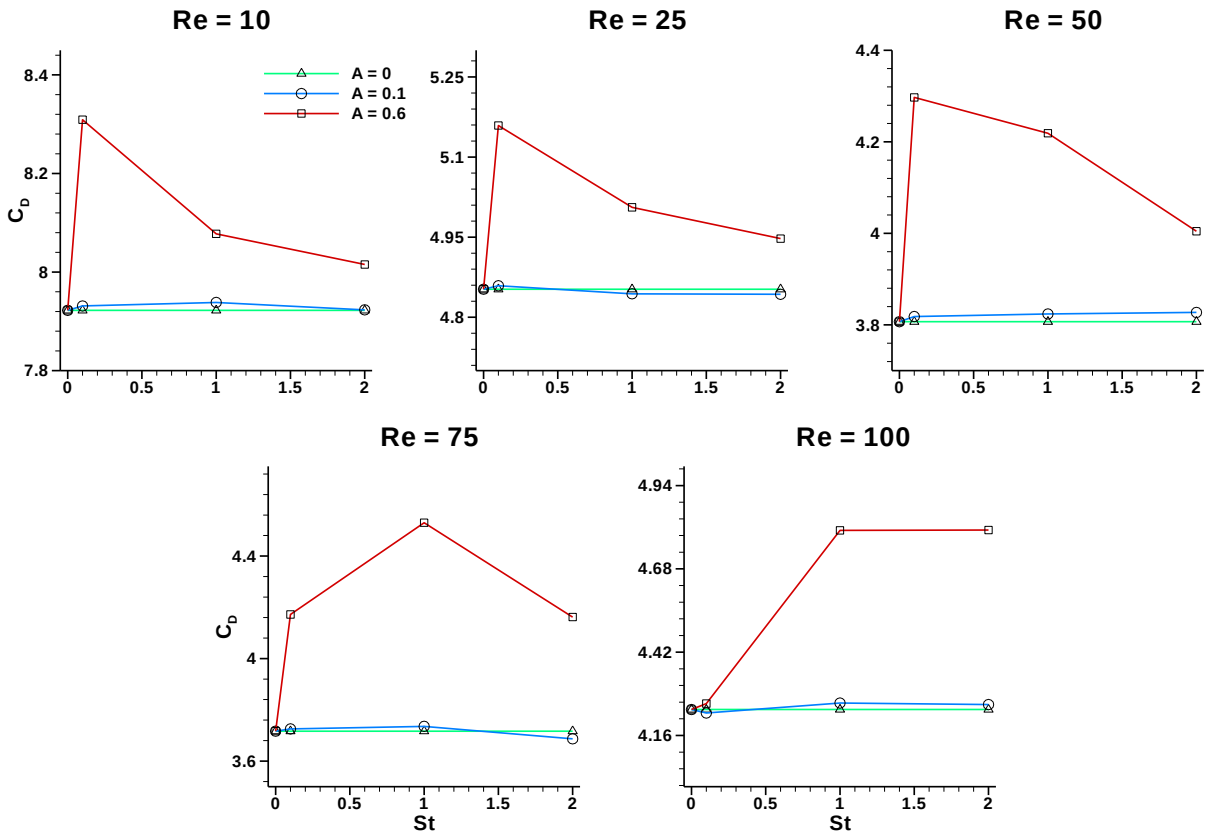

FIGURE 22. Variation of total drag coefficient (C_D) with A and St at different Re

4.5. Average Nusselt number

The parameter indicating heat transfer quantitatively is expressed as Nusselt number. Figure 23 reveals the effect of (forcing) Strouhal number (*St* = 0, 0.1, 1 and 2) as well as the oscillation amplitude (*A* = 0, 0.1 and 0.6) over the average *Nu* values for the semi-circular cylinder at different Reynolds number (Re = 10, 25, 50, 75 and 100). It can be inferred from the figure that overall rate of heat transfer increased as Re grew for constant pairs of *A* and *St*. Also, for a constant *St* value at $\mathrm{Re} \leq 25$, the Nusselt number grew with the amplitude. In other words, *Nu* in case of pulsating flow is larger than that in case of flow which is steady, for $\mathrm{Re} \leq 25$. However for $\mathrm{Re} \geq 50$, the Nusselt numbers at *A* = 0.6 were smaller than that at *A* = 0.1, particularly for *St* = 0.1, thus indicating non-monotonic trend with respect to both *St* and *A* for these Re. It is noteworthy that amongst all the cases studied, an appreciable amount of augmentation is observed when *St*=1 and *A*=0.6 (with respect to the case of non pulsating flow i.e. *St*=0). A maximum of around 10% augmentation in Nusselt number is identified.

For higher Re, it is noteworthy that much in accordance to the case of complete cylinder (Al-Sumaily and Thompson [7]), the effect of *A* over *Nu* considerably vanishes at lower *St* for semi-circular cylinder as well. Again, the plots show peaks of *Nu* at certain values of *St*. Above and below this value, *Nu* is lower. It is noteworthy that heat transfer in the case of confined semi-circular cylinder is for sure greater than that in case of confined circular cylinder for the discussed ranges of parameters of interest.

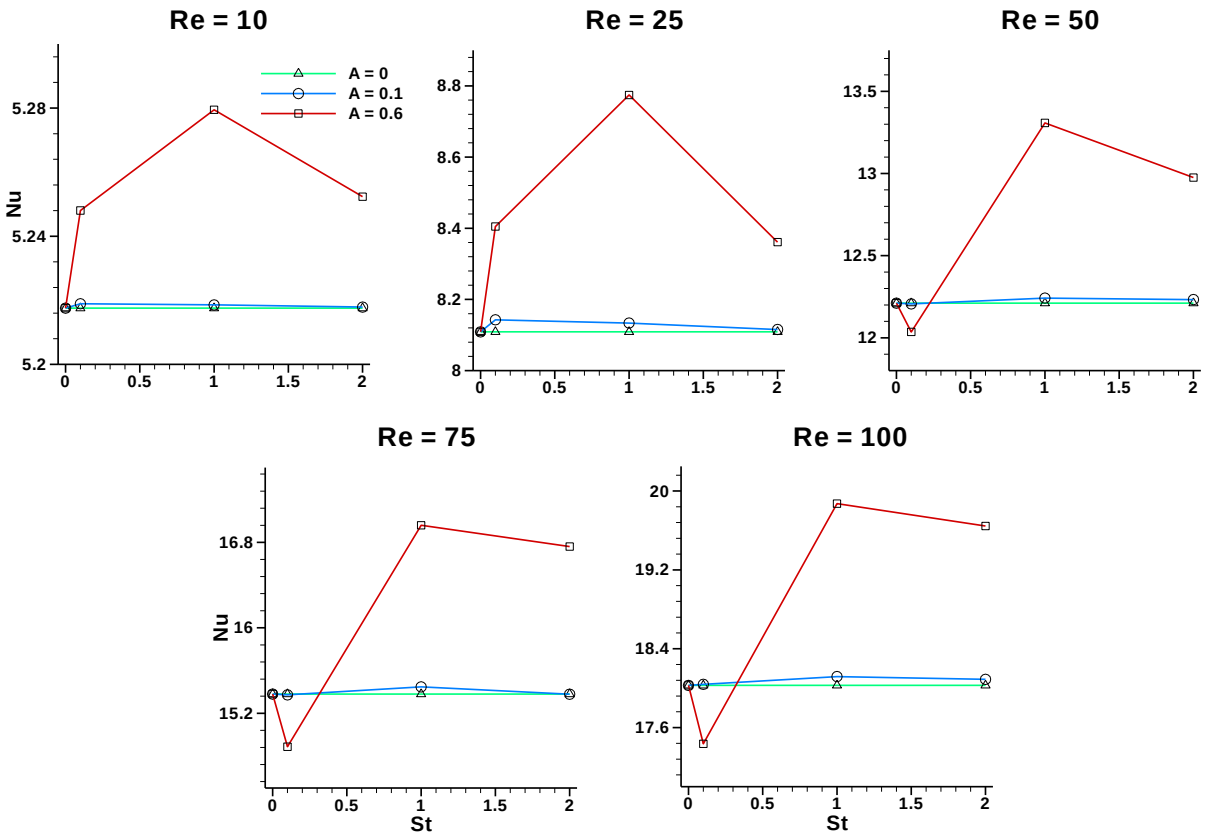

FIGURE 23. Variation of Nusselt number (Nu) with *A* and *St* at different Re

CHAPTER 5. CONCLUSIONS

5.1. Conclusions

The study numerically investigates the influence of pulsatile flow around a (heated) confined semi-circular cylinder in terms of fluid flow as well as heat transfer characteristics. The parameters of interest taken into consideration ranged as follows: Re = 10-100; *St* = 0-2; A = 0-0.6 for $\beta = 25\%$ and Pr = 7. Resolution studies were performed to make the numerical computations independent of domain as well as mesh size effects. Also time step study was performed. Extensive computations were carried out for the set of parameters under study in order to evaluate the Nusselt number, the drag coefficient and others. The nature of fluid flow was observed for all the cases considered. It was identified that pulsatile inlet flow velocities eventually make heat transfer augmentation possible. In general for a given Re, both the amplitude range as well as the *St* values determined the amount of the augmentation in heat transfer. A maximum of around 22% and 10% augmentation was identified in coefficient of drag and Nusselt number, respectively. The time histories of *Nu* and C_D were examined. The thermal and streamline contours were produced, finally.

5.2. Scope for future work

Significant amount of scope exists in direction of extending the findings of present research. Some of the noteworthy aspects where the research could be directed are listed here:

- A similar research can be performed for higher range of Reynolds number and/or different sets of Prandtl number.
- Determination of the vortex shedding frequency and the transition regime for the same work.
- A similar study could be performed for the case of multiple semi-circular cylinders mounted in a set of different arrangements. Alternately, the shape of cylinder could be altered to a triangular or square (or any other) cylinder for an entirely new research.
- The research could also take into account the case of oscillating cylinder(s).

REFERENCES

1. Chandra, A., & Chhabra, R. P. (2011). Flow over and forced convection heat transfer in Newtonian fluids from a semi-circular cylinder. *International Journal of Heat and Mass Transfer*, *54*(1), 225-241.
2. Chandra, A., & Chhabra, R. P. (2011). Momentum and heat transfer characteristics of a semi-circular cylinder immersed in power-law fluids in the steady flow regime. *International Journal of Heat and Mass Transfer*, *54*(13), 2734-2750.
3. Chandra, A., & Chhabra, R. P. (2013). Momentum and heat transfer from a semi-circular cylinder to power-law fluids in the vortex shedding regime. *Numerical Heat Transfer, Part A: Applications*, *63*(7), 489-510.
4. Kumar, A., & Dhiman, A. (2015). Laminar Flow and Heat Transfer Phenomena Across a Confined Semicircular Bluff Body at Low Reynolds Numbers. *Heat Transfer Engineering*, *36*(18), 1540-1551.
5. Kumar, A., Dhiman, A., & Baranyi, L. (2015). CFD analysis of power-law fluid flow and heat transfer around a confined semi-circular cylinder. *International Journal of Heat and Mass Transfer*, *82*, 159-169.
6. Qamar, A., Seda, R., & Bull, J. L. (2011). Pulsatile flow past an oscillating cylinder. *Physics of Fluids (1994-present)*, *23*(4), 0419031-04190313.
7. Al-Sumaily, G. F., & Thompson, M. C. (2013). Forced convection from a circular cylinder in pulsating flow with and without the presence of porous media. *International Journal of Heat and Mass Transfer*, *61*, 226-244.
8. Lin, Y. C., Brant, D. O., Bartlett, R. H., Hirschl, R. B., & Bull, J. L. (2006). Pulsatile flow past a cylinder: An experimental model of flow in an artificial lung. *ASAIO Journal*, *52*(6), 614-623.
9. Lin, Y. C., Khanafer, K. M., Bartlett, R. H., Hirschl, R. B., & Bull, J. L. (2011). An investigation of pulsatile flow past two cylinders as a model of blood flow in an artificial lung. *International Journal of Heat and Mass Transfer*, *54*(15), 3191-3200.
10. Zierenberg, J. R., Fujioka, H., Suresh, V., Bartlett, R. H., Hirschl, R. B., & Grotberg, J. B. (2006). Pulsatile flow and mass transport past a circular cylinder. *Physics of Fluids (1994-present)*, *18*(1), 0131021-01310215.

11. Zierenberg, J. R., Fujioka, H., Hirschl, R. B., Bartlett, R. H., & Grotberg, J. B. (2007). Pulsatile blood flow and oxygen transport past a circular cylinder. *Journal of Biomechanical Engineering*, *129*(2), 202-215.
12. Konstantinidis, E., & Balabani, S. (2008). Flow structure in the locked-on wake of a circular cylinder in pulsating flow: Effect of forcing amplitude. *International Journal of Heat and Fluid Flow*, *29*(6), 1567-1576.
13. Liang, C., & Papadakis, G. (2007). Large eddy simulation of pulsating flow over a circular cylinder at subcritical Reynolds number. *Computers & Fluids*, *36*(2), 299-312.
14. Iwai, H., Mambo, T., Yamamoto, N., & Suzuki, K. (2004). Laminar convective heat transfer from a circular cylinder exposed to a low frequency zero-mean velocity oscillating flow. *International Journal of Heat and Mass Transfer*, *47*(21), 4659-4672.
15. Zhao, M., & Cheng, L. (2014). Two-dimensional numerical study of vortex shedding regimes of oscillatory flow past two circular cylinders in side-by-side and tandem arrangements at low Reynolds numbers. *Journal of Fluid Mechanics*, *751*, 1-37.
16. Tong, F., Cheng, L., Zhao, M., & An, H. (2015). Oscillatory flow regimes around four cylinders in a square arrangement under small and conditions. *Journal of Fluid Mechanics*, *769*, 298-336.
17. Zdravkovich, M. M. (2003). *Flow around Circular Cylinders: Applications*, Vol. 2, Oxford University press.
18. Bijjam, S., & Dhiman, A. K. (2012). CFD analysis of two-dimensional non-Newtonian power-law flow across a circular cylinder confined in a channel. *Chemical Engineering Communications*, *199*(6), 767-785.
19. Abbassi, H., Turki, S., & Nasrallah, S. B. (2001). Numerical investigation of forced convection in a plane channel with a built-in triangular prism. *International Journal of Thermal Sciences*, *40*(7), 649-658.
20. Srikanth, S., Dhiman, A. K., & Bijjam, S. (2010). Confined flow and heat transfer across a triangular cylinder in a channel. *International Journal of Thermal Sciences*, *49*(11), 2191-2200.

21. Agarwal, R., & Dhiman, A. (2014). Flow and heat transfer phenomena across two confined tandem heated triangular bluff bodies. *Numerical Heat Transfer, Part A: Applications*, *66*(9), 1020-1047.
22. Rasool, T., Dhiman, A., & Parveez, M. (2015). Cross-buoyancy mixed convection around a confined triangular bluff body. *Numerical Heat Transfer, Part A: Applications*, *67*(4), 454-475.
23. Dhiman, A. K. (2009). Heat transfer to power-law dilatant fluids in a channel with a built-in square cylinder. *International Journal of Thermal Sciences*, *48*(8), 1552-1563.
24. Bharti, R. P., Chhabra, R. P., & Eswaran, V. (2007). Effect of blockage on heat transfer from a cylinder to power law liquids. *Chemical Engineering Science*, *62*(17), 4729-4741.